Atmospheric Environment 85 (2014) 123–138

Contents lists available at ScienceDirect

Atmospheric Environment

journal homepage: www.elsevier.com/locate/atmosenv

Impacts of aerosols on surface-layer ozone concentrations in China through heterogeneous reactions and changes in photolysis rates☆

Sijia Lou [a,b], Hong Liao [a,*], Bin Zhu [c]

[a] State Key Laboratory of Atmospheric Boundary Layer Physics and Atmospheric Chemistry (LAPC), Institute of Atmospheric Physics, Chinese Academy of Sciences, Beijing 100029, China
[b] Graduate University of Chinese Academy of Sciences, Beijing 100049, China
[c] Department of Atmospheric Physics, Nanjing University of Information Science & Technology, Nanjing 210044, China

HIGHLIGHTS

- We have examined the spatial and temporal variations of aerosol impacts on O_3.
- We have quantified the role of each and all heterogeneous reactions.
- Heterogeneous reactions reduce O_3 in eastern China by 10–18% on an annual mean basis.
- Concentration of O_3 in Pearl River Delta is most sensitive to the impacts of aerosols.

ARTICLE INFO

Article history:
Received 6 October 2013
Received in revised form
1 December 2013
Accepted 4 December 2013

Keywords:
Tropospheric ozone
Aerosols
Heterogeneous reactions
Photolysis rates

ABSTRACT

We quantify the impacts of aerosols on distributions and concentrations of O_3 over China through heterogeneous reactions and changes in photolysis rates using the global chemical transport model GEOS-Chem. Aerosols considered include sulfate, nitrate, ammonium, organic carbon, and black carbon. Consideration of the impacts of aerosols improves the simulated O_3 concentrations in China; the averaged biases in simulated O_3 concentrations in China are +9% and +33% with and without the impacts of aerosols, respectively. The impacts of heterogeneous reactions on O_3 are simulated to exhibit large spatial and temporal variations, and those of aerosols through altering photolysis rates are simulated to be small. Accounting for hydrolysis of N_2O_5, irreversible absorption of NO_2 and NO_3 on wet aerosols, and the uptake of HO_2 by aerosols, O_3 concentrations are simulated to decrease by 8–12 ppbv in northern China and to increase by 3–6 ppbv in southern China in winter, and reductions in O_3 of exceeding 6 ppbv are simulated in a large fraction of China in other seasons. With the assumed uptake coefficients in this work, the hydrolysis of N_2O_5 is simulated to have a dominant role in reducing O_3 concentrations all over China, as a result of the large reductions in NO_x in the lower to middle troposphere in the northern mid-latitudes. On the contrary, the absorption of NO_2 and NO_3 is found to increase O_3 concentrations by 3–10 ppbv in eastern China in winter because of the increases in chemical production of O_3 in the VOC-limited regions. The impact of aerosols on O_3 concentration through heterogeneous reactions is characterized in this work by the ratio of change in O_3 concentration to local $PM_{2.5}$ level (ROP = $\Delta[O_3]/[PM_{2.5}]$). The locations of maximum reductions in O_3 are not necessarily the places of maximum aerosol concentrations; the annual mean values of ROP are calculated to be −0.14, −0.17, −0.27, and −0.16 ppbv $(\mu g\ m^{-3})^{-1}$ over the heavily polluted regions of Beijing–Tianjin–Tanggu, Yangtze River Delta, Pearl River Delta, and Sichuan Basin, respectively. Values of ROP are determined by both local heterogeneous reactions and transport of O_3 from surrounding areas.

1. Introduction

Tropospheric O_3 and aerosols are major air pollutants in the atmosphere that have adverse effects on human health, crops, plants, and atmospheric visibility. They have also made significant contributions to radiative forcing of climate since preindustrial time (Intergovernmental Panel on Climate Change (IPCC), 2007).

* Corresponding author.
E-mail address: hongliao@mail.iap.ac.cn (H. Liao).

1352-2310/$ – see front matter © 2013 The Authors. Published by Elsevier Ltd. All rights reserved.
http://dx.doi.org/10.1016/j.atmosenv.2013.12.004

Concentrations of tropospheric O_3 and aerosols are coupled through the formation and growth of aerosols, heterogeneous reactions, and aerosol-induced changes in photolysis rates. With the rapid urbanization and economic development, observed aerosol concentrations are especially high in China (Cao et al., 2007; Andreae et al., 2008; Gu et al., 2011; Zhang et al., 2012), suggesting that aerosols in China can have large impacts on O_3 concentrations.

Previous global and regional modeling studies have shown that aerosols influence O_3 concentrations in China by heterogeneous reactions. Liao and Seinfeld (2005) found that simulated surface-layer O_3 concentrations over eastern China can be reduced by 25–30% due to heterogeneous reactions on sulfate (SO_4^{2-}), nitrate (NO_3^-), ammonium (NH_4^+), organic carbon (OC), sea salt, and mineral dust aerosols, accounting for the hydrolysis of N_2O_5, irreversible absorption of NO_3, NO_2, and HO_2 on wetted aerosol surfaces, mineral dust uptake of SO_2, O_3, and HNO_3, as well as the sea salt uptake of SO_2 in a coupled global chemistry–aerosol–climate model based on the Goddard Institute for Space Studies (GISS) GCM II' at 4°×5° resolution. Tie et al. (2005) used a coupled global aerosol–chemistry model, Model for Ozone and Related Chemical Tracers (MOZART) with a horizontal resolution of 2.8°×2.8°, to study the impacts of heterogeneous reactions on O_3 by considering the heterogeneous reactions of HO_2 and CH_2O on sulfate aerosol as well as the uptake of O_3 on black carbon (BC). They found that O_3 concentrations were reduced by 10–15% and 5–10% in eastern China in winter and summer, respectively. Pozzoli et al. (2008) showed that surface-layer O_3 concentrations were reduced by 18–23% over the Transport and Chemical Evolution over the Pacific (TRACE-P) region in March of 2001, when all the heterogeneous reactions listed in Liao and Seinfeld (2005) were considered in the coupled ECHAM5-HAMMOZ model with a spatial resolution of 2.8°×2.8°. Xu et al. (2012) used the Community Multi-scale Air Quality Model (CMAQ) with a horizontal resolution of 4 km to study the impacts of heterogeneous reactions on O_3 during a high O_3 episode occurred in Beijing in June 26–27, 2000. They reported that the impacts of heterogeneous reactions on O_3 depend on the local NO_x/VOC ratio. For example, the absorption of NO_2 by aerosols was found to increase O_3 at noon by 4–20 ppbv (or 3–14%) in VOC-limited urban areas and to decrease O_3 by 4–10 ppbv (or 3–7%) in NO_x-limited sub-urban areas.

Previous modeling studies have also shown that aerosols can influence O_3 in China by altering photolysis rates. Tang et al. (2004) found that O_3 concentrations were reduced by 0.1–0.8% in northeastern China during the dust event of April 4–14, 2001, by using the Sulfur Transport and Emissions Model (STEM) with a spatial resolution of 80 km, as a result of the dust-induced changes in photolysis rates. Tie et al. (2005) showed that surface-layer photolysis rates $J(O_3)$ and $J(NO_2)$ in eastern China were reduced, respectively, by 20–30% and 10–30% in winter as well as 5–20% and 1–10% in summer, leading to reductions in surface-layer O_3 concentrations by 2–4% in winter and less than 2% in summer. Li et al. (2011) used a regional Nested Air Quality Prediction Model System (NAQPMS) with a horizontal resolution of 81 km to estimate the changes in photolysis rates in central eastern China by SO_4^{2-}, NO_3^-, NH_4^+, OC, BC, and mineral dust aerosols during June 1–12, 2006. They reported that aerosols reduced daytime average $J(O^1D)$ in layers below 1 km, 1–3 km, and 3–10 km by 53.3%, 37.2%, and 20.9%, respectively, which led to changes in O_3 concentrations by −5.4%, −3.8% and 0.1% in those three layers, respectively.

Few previous studies examined the combined impacts of aerosols on O_3 by both heterogeneous reactions and aerosol-induced changes in photolysis rates. Martin et al. (2003) considered the heterogeneous reactions of HO_2, NO_2, NO_3, and N_2O_5 as well as the optical properties of SO_4^{2-}, BC, OC, sea salt, and mineral dust in the global three-dimensional Goddard Earth Observing System chemical transport model (GEOS-Chem) at 2°×2.5° resolution, and found that O_3 concentrations were reduced by 5–10 ppbv (10–15%) over northeastern China in March and by up to 5 ppbv over North China Plain in August of 1997. This study, however, excluded the impacts of hydrolysis of N_2O_5, did not consider NO_3^- and NH_4^+ aerosols in the calculation of photolysis rates, and did not examine the spatial and temporal variations of the impacts of aerosols on O_3 concentrations in China.

The studies cited above underscored the important impacts of aerosols on tropospheric O_3 in China. The goal of this study is to examine systematically the impacts of aerosols on O_3 concentrations in China using the nested-grid version of the GEOS-Chem model with a horizontal resolution of 0.5° latitude by 0.667° longitude driven by the assimilated meteorological fields. We pay special attention to (1) the spatial and temporal variations of the impacts of aerosols on O_3, and (2) the role of each and all heterogeneous reactions. We focus especially on the impacts in four heavily polluted regions in China, including Beijing–Tianjin–Tanggu (BTT, 35°–40°N, 114°–120°E), Yangtze River Delta (YRD, 29.5°–32.5°N, 118°–122°E), Pearl River Delta (PRD, 21°–23.5°N, 112–116°E), and Sichuan Basin (SCB, 28°–31.5°N, 102.5°–107.5°E).

The description of model and numerical experiments is presented in Section 2. Simulated concentrations aerosols and O_3 are presented and evaluated in Section 3. Sections 4 and 5 examine, respectively, the impacts of aerosols on concentrations of O_3 by heterogeneous reactions alone and by changes in photolysis rates alone. The combined effects are presented in Section 6 and the associated model uncertainties are discussed in Section 7.

2. Model description

2.1. GEOS-Chem model

We simulate concentrations of O_3 and aerosols using the one-way nested-grid capability of the global chemical transport model GEOS-Chem (version 9.1.2, http://acmg.seas.harvard.edu/geos/). GEOS-Chem is driven by the GEOS-5 assimilated meteorological fields from the Goddard Earth Observing System of the NASA Global Modeling Assimilation Office. The nested domain for Asia (70–150°E, 10°S–55°N) has a horizontal resolution of 0.5° latitude by 0.667° longitude and 47 vertical layers up to 0.01 hPa. Tracer concentrations at the lateral boundaries are provided by a global GEOS-Chem simulation at 4° latitude by 5° longitude horizontal resolution and updated in the nested-grid model every 3 h (Chen et al., 2009).

The GEOS-Chem model has fully coupled O_3–NO_x–hydrocarbon chemistry and aerosols including $SO_4^{2-}/NO_3^-/NH_4^+$ (Park et al., 2004; Pye et al., 2009), OC and BC (Park et al., 2003), sea salt (Alexander et al., 2005), and mineral dust (Fairlie et al., 2007). Tropospheric O_3 is simulated with about 80 species and over 300 chemical reactions (Bey et al., 2001). Partitioning of nitric acid and ammonia between the gas and aerosol phases is calculated by ISORROPIA II (Fountoukis and Nenes, 2007). SOA formation considers the oxidation of isoprene (Henze and Seinfeld, 2006), monoterpenes and other reactive VOCs (ORVOCs) (Liao et al., 2007), and aromatics (Henze et al., 2008). The mineral dust and sea salt aerosols are not considered in this study.

2.2. Heterogeneous reactions on aerosols

Heterogeneous reactions on anthropogenic aerosols in the GEOS-Chem model are listed in Table 1, including hydrolysis of N_2O_5 (Evans and Jacob, 2005), irreversible absorption of NO_3 and NO_2 on wet aerosols (Jacob, 2000), and the uptake of HO_2 by

Table 1
Uptake coefficients for heterogeneous reactions on aerosols surfaces.

	Reactions	Aerosols	Uptake coefficients	References
R1	$N_2O_5 \rightarrow 2HNO_3$	Sulfate/nitrate/ammonium	γ_{N2O5}[a]	Evans and Jacob (2005)
	$N_2O_5 \rightarrow 2HNO_3$	Black carbon	0.005	Sander et al. (2003)
	$N_2O_5 \rightarrow 2HNO_3$	Organic carbon	0.03 (RH $\geq$ 57%); RH $\times$ 5.2 $\times$ 10^{-4} (RH $<$ 57%)	Thornton et al. (2003)
R2	$NO_3 \xrightarrow{}HNO_3$	Wet aerosols[b]	0.001	Jacob (2000)
R3	$NO_2 \rightarrow 0.5HONO + 0.5HNO_3$	Wet aerosols[b]	0.0001	Jacob (2000)
R4	$HO_2 \rightarrow 0.5H_2O_2$	Sulfate/nitrate/ammonium[c]	0.07	Thornton et al. (2008)
	$HO_2 \rightarrow 0.5H_2O_2$	Wet aerosols[d]	γ_{HO2}[d]	Thornton et al. (2008)

[a] $\gamma_{N_2O_5} = 10^{\beta(T)} \times (2.79 \times 10^{-4} + 1.3 \times 10^{-4} \times RH - 3.43 \times 10^{-6} \times RH^2 + 7.52 \times 10^{-8} \times RH^3)$; $\beta(T) = -4 \times 10^{-2} \times (T - 294)$ for $T \geq 282$ K; $\beta(T) = 0.48$ for $T < 282$ K.
[b] Sulfate, nitrate, ammonium, and organic carbon aerosols are considered to be wet when RH $\geq$ 50.
[c] Sulfate/nitrate/ammonium aerosols in the boundary layer of continents.
[d] $\gamma_{HO_2} = \frac{4F_R}{\omega X_g}$; $F_R = k_{mt}\left(X_g - \frac{N_{AV}}{1000 H_{eff} RT} X_{aq}\right)\frac{3}{r_p}$; $k_{mt} = \frac{\alpha\omega}{4}$; k_{mt} is the rate constant for interfacial mass transport in the free molecular regime, ω is the mean molecular speed of HO_2, X_{aq} is the steady state concentration of HO_2 at the aerosol surface, H_{eff} is the effective Henry's law constant, R is the universal gas constant, T is temperature, N_{AV} is Avagadro's number, r_p is particle radius, and X_g is the gas-phase number density of HO_2.

aerosols (Thornton et al., 2008). Hydrolysis of N_2O_5 on wetted aerosol surfaces is calculated as a function of aerosol type, relative humidity, and temperature (Table 1), following Evans and Jacob (2005). For the absorption of NO_2 and NO_3 by wet aerosols, γ_{NO_2} is in the range of 10^{-4}–10^{-3} on the basis of laboratory studies (DeMore et al., 1997; Harrison and Collins, 1998), and the measured γ_{NO_3} is in the range of 2×10^{-4}–10^{-2} (Exner et al., 1992, 1994; Rudich et al., 1996). In the GEOS-Chem model, the uptake coefficients γ_{NO_2} and γ_{NO_3} are assumed to be 0.0001 and 0.001 (Jacob, 2000), respectively. The uptake coefficient γ_{HO_2} is calculated as a function of temperature for all aerosol species except that a value of 0.07 is specified for $SO_4^{2-}/NO_3^-/NH_4^+$ aerosols in the continental boundary layer (Thornton et al., 2008). The uptake coefficient of N_2O_5 ($\gamma_{N_2O_5}$) was used in previous modeling studies and led to improved agreement between simulated and observed O_3 concentrations (Evans and Jacob, 2005; Pozzoli et al., 2008). It should be mentioned that Mao et al. (2013) suggested a new γ_{HO_2} of 1.0 to produce H_2O in the presence of dissolved Cu and Fe; the impact of the assumed γ_{HO_2} on simulated O_3 concentrations will be discussed in Section 7.

2.3. Gas-phase photolysis

Rates of 55 photolysis reactions in the GEOS-Chem model are computed every time step using the Fast-J radiative transfer code (Wild et al., 2000; Bian and Prather, 2002), which has 6 wavelength channels covering 289–412.45 nm and accounts for absorption by O_2 and O_3, Rayleigh scattering, and radiative effects of clouds and aerosols. We consider the radiative impacts of $SO_4^{2-}/NO_3^-/NH_4^+$, OC, and BC aerosols on photolysis rates in this study. The optical properties of aerosols are calculated as described in Martin et al. (2003) and Drury et al. (2010).

2.4. Emissions

Global emissions of O_3 precursors, aerosol precursors, and aerosols in the GEOS-Chem model generally follow Park et al. (2003, 2004), in which anthropogenic emissions of CO, NO_x, SO_2, and NMVOCs in the Asian domain have been overwritten by David Streets' 2006 emission inventory (http://mic.greenresource.cn/intex-b2006). Emissions of NH_3 are taken from Streets et al. (2003) and a scaling factor is used to reduce the total NH_3 emission in China from 13.5 Tg yr^{-1} in Streets et al. (2003) to the most recent estimate of 9.8 Tg yr^{-1} by Huang et al. (2012). Table 2 summarizes the annual emissions of NO_x, CO, NMVOCs, SO_2, NH_3, OC, and BC in eastern China (110–126°E, 20–50°N).

Monthly variations of SO_2, NO_x, NH_3, OC, and BC emissions are shown in Fig. 1, which follow those in Zhang et al. (2010) and Wang et al. (2013). Because of the winter energy use, emissions of CO, SO_2, OC, and BC are the highest in winter months. Emissions of NMVOCs are the highest in July, because biogenic emissions are the maximum at high temperatures (Guenther et al., 2006). The emissions of NH_3 are the highest in June as a result of the agriculture practice and high temperatures (Wang et al., 2013).

2.5. Numerical experiments

We perform the following GEOS-Chem simulations to examine the relative importance and the combined impacts of

Table 2
Annual emissions of ozone precursors, aerosol precursors, and aerosols in eastern China (20°–50°N, 110°–126°E).

Species	Eastern China
NO_x (Tg N yr^{-1})	
Aircraft	0.01
Anthropogenic	4.88
Biomass burning	0.01
Fertilizer	0.09
Lightning	0.16
Soil	0.16
Total	5.32
CO (Tg CO yr^{-1})	
Anthropogenic	130.89
Biomass burning	1.11
Total	132.00
NMVOCs (Tg C yr^{-1})	
Anthropogenic	6.71
Biomass burning	0.05
Biogenic	9.50
Total	16.26
SO_2 (Tg S yr^{-1})	
Aircraft	0.002
Anthropogenic	11.55
Biomass burning	0.004
No_eruption volcanoes	0.21
Ship	0.11
Total	11.88
NH_3 (Tg N yr^{-1})	
Anthropogenic	6.64
Natural	0.41
Biomass burning	0.02
Biofuel	0.23
Total	7.29
OC (Tg C yr^{-1})	
Anthropogenic	0.74
Biomass burning	0.06
Biofuel	0.99
Biogenic	0.29
Total	2.08
BC (Tg C yr^{-1})	
Anthropogenic	0.68
Biomass burning	0.007
Biofuel	0.27
Total	0.95

heterogeneous reactions and the aerosol-induced changes in photolysis rates on O_3 concentrations in China (Table 3):

(1) CTRL: The control simulation of O_3 with all heterogeneous reactions listed in Table 1 and the effect of aerosols on photolysis rates.
(2) NOALL: The same as the CTRL simulation but without the heterogeneous reactions and the effect of aerosols on photolysis rates.
(3) HETG: The simulation of O_3 with heterogeneous reactions but without the effect of aerosols on photolysis rates. A set of four simulations are performed to quantify the role of each heterogeneous reaction: 1) HETG_All has all the heterogeneous reactions listed in Table 1; 2) HETG_noN_2O_5 is the same as HETG_All except that it does not consider the hydrolysis of N_2O_5; 3) HETG_noNO_x is the same as HETG_All except that it does not account for the aerosol uptake of NO_2 and NO_3; and 4) HETG_noHO_2 is the same as HETG_All but does not account for the aerosol uptake of HO_2.
(4) EMIS: Sensitivity studies to examine how the impacts of aerosols (through heterogeneous reactions and changes in photolysis rates) on O_3 change with aerosol concentrations. Emissions of OC are increased by 100–400% over China based on the comparisons of simulated OC concentrations in the CTRL simulation with measurements (see Section 3.3).

The differences in simulated O_3 between CTRL and NOALL simulations represent the combined impacts of heterogeneous reactions and the aerosol-induced changes in photolysis on O_3 concentrations. The differences between CTRL and HETG_All represent the impacts of aerosols on O_3 by altering photolysis rates. The roles of all and each of heterogeneous reactions can be quantified by (HETG_All–NOALL), (HETG_All–HETG_noN_2O_5), (HETG_All–HETG_noNO_x), and (HETG_All–HETG_noHO_2), respectively. All simulations are integrated for the period of 1 January to 31 December of year 2005 after a 6-month model spin up.

3. Simulated concentrations of aerosols and O_3 in China

3.1. Aerosols

Fig. 2 shows the simulated seasonal mean surface-layer concentrations of SO_4^{2-}, NO_3^-, NH_4^+, BC, OC, and $PM_{2.5}$ (sum of SO_4^{2-}, NO_3^-, NH_4^+. BC, and OC) in China from the CTRL simulation. Sulfate concentrations of 15–25 μg m^{-3} are simulated over the SCB throughout the year and over the BTT in JJA and SON. Concentrations of NO_3^- and NH_4^+ in DJF and SON are higher than those in MAM and JJA, which can be explained by the low temperatures that favor ammonium nitrate formation. Concentrations of BC and OC over eastern China are the highest in DJF, with the maximum values of 5–10 and 10–15 μg m^{-3}, respectively, as a result of the winter heating. On an annual mean basis, nitrate is simulated to be the most abundant aerosol species over eastern China, followed by SO_4^{2-}, NH_4^+ OC, and BC.

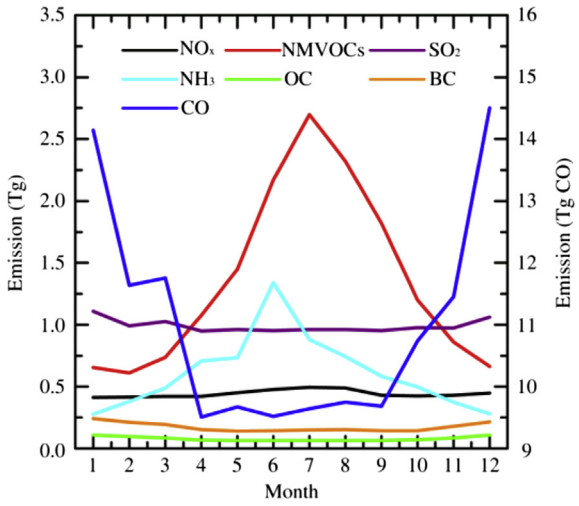

Fig. 1. Monthly variations in emissions of NO_x (Tg N $month^{-1}$), NMVOCs (Tg C $month^{-1}$), SO_2 (Tg S $month^{-1}$), NH_3 (Tg N $month^{-1}$), OC (Tg C $month^{-1}$), BC (Tg C $month^{-1}$), and CO (Tg CO $month^{-1}$) over eastern China (20°–50°N, 110°–126°E). Emissions shown are the total values of anthropogenic and natural sources listed in Table 2. The left axis is for NO_x, NMVOCs, SO_2, and NH_3, and the right axis is for CO.

3.2. Ozone

Fig. 2 also shows the simulated seasonal mean surface-layer concentrations of O_3 in the CTRL simulation with all heterogeneous reactions and the effect of aerosols on photolysis rates. Concentrations of O_3 in eastern China are the lowest in December–January–February (DJF) because of the weak photochemistry. Concentrations of O_3 in eastern China in MAM and SON are in the ranges of 40–55 ppbv and 35–50 ppbv, respectively. The maximum O_3 concentrations over eastern China are simulated to be 60–75 ppbv in JJA. Note that the high O_3 concentrations of exceeding 70 ppbv over the Tibet Plateau in MAM result from the transport of O_3 from the stratosphere to troposphere (Wild and Akimoto, 2001).

3.3. Comparisons of simulated concentrations with measurements

Simulated concentrations of O_3 and aerosols in China using the one-way nested-grid capability of the GEOS-Chem have been evaluated in studies of Wang et al. (2011, 2013) and Fu et al. (2012). Wang et al. (2011) demonstrated that the model captures well the magnitude and seasonal variation of surface-layer concentrations and column burdens of O_3 in China. Wang et al. (2013) found that

Table 3
Experimental design.

Experiments	Heterogeneous reactions	Effect of aerosols on photolysis rates	Emissions
CTRL	With all heterogeneous reactions listed in Table 1	Yes	Default (with emissions described in Section 2.4)
NOALL	With no heterogeneous reactions	No	Default
HETG_All	With all heterogeneous reactions listed in Table 1	No	Default
HETG_noN_2O_5	With all heterogeneous reactions listed in Table 1 except for the uptake of N_2O_5	No	Default
HETG_noNO_x	With all heterogeneous reactions listed in Table 1 except for the absorption of NO_2 and NO_3	No	Default
HETG_noHO_2	With all heterogeneous reactions listed in Table 1 except for the uptake of HO_2	No	Default
EMIS	With all heterogeneous reactions listed in Table 1	Yes	Default but with increases in OC emissions by 2–5 times

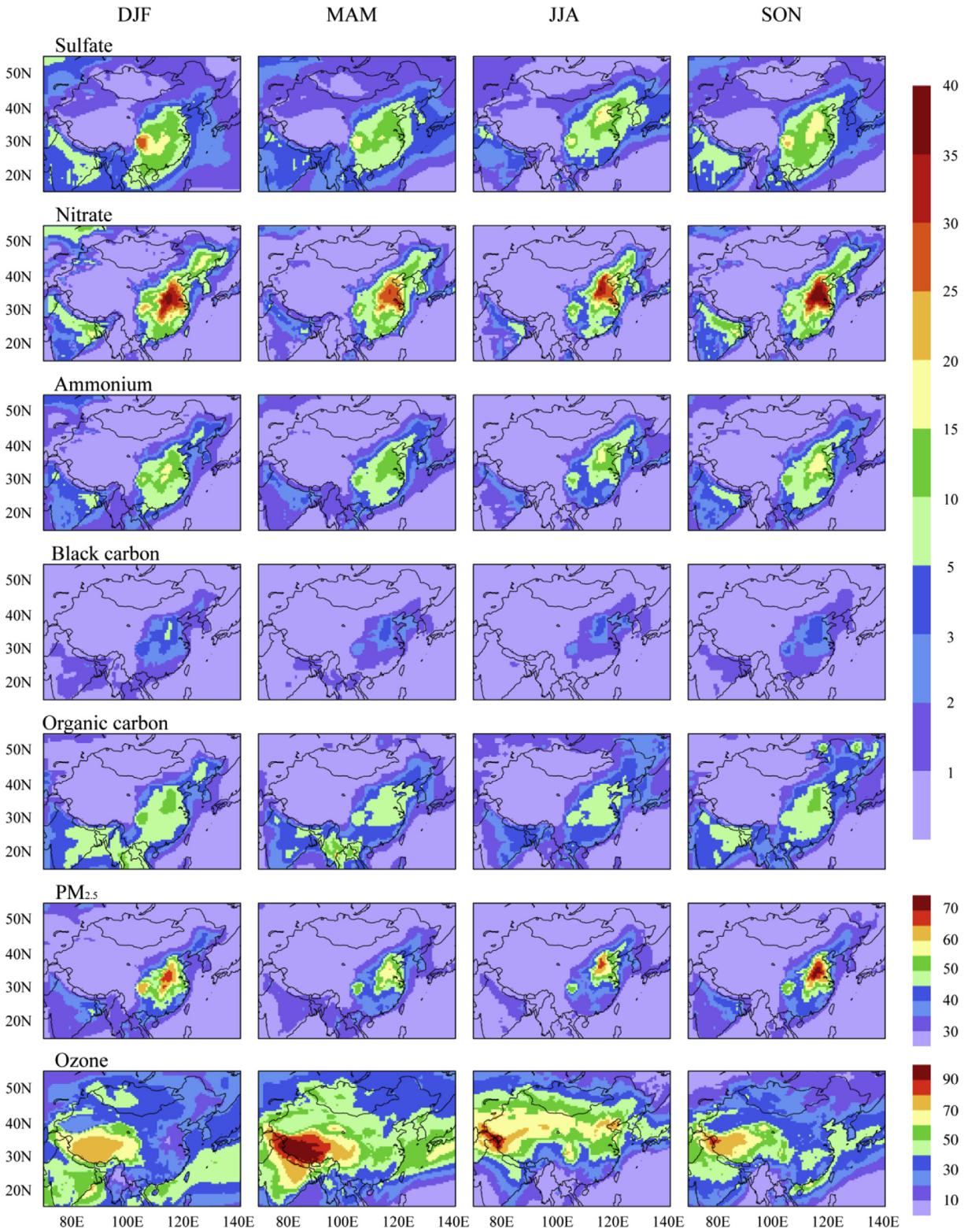

Fig. 2. Simulated seasonal mean surface-layer concentrations of sulfate, nitrate, ammonium, BC, OC, $PM_{2.5}$, and O_3 in the CTRL simulation. Units are μg m^{-3} for aerosols and ppbv for O_3.

simulated concentrations of SO_4^{2-}, NO_3^-, NH_4^+ at 22 sites in East Asia exhibited annual biases of −10%, +31%, and +35%, respectively, and Fu et al. (2012) reported that the simulated annual mean concentrations of BC and OC averaged over rural and background sites were underestimated by 56% and 76%, respectively.

The major purpose of model evaluation here is to see whether the version of the GEOS-Chem model we use can capture the magnitude of the observed aerosols and O_3. The seasonal mean measured concentrations of SO_4^{2-}, NO_3^-, NH_4^+, BC, and OC were taken from Zhang et al. (2012), which were PM_{10} mass

concentrations measured at 7 urban sites and 7 remote sites around China over 2006–2007 (Fig. 3(a)). The observed concentrations listed in Zhang et al. (2012) are multiplied by 0.6 to convert PM_{10}–$PM_{2.5}$ for model evaluation following the suggestions in Zhang et al. (2002). The scatter plots of simulated versus observed seasonal mean concentrations of SO_4^{2-}, NO_3^-, NH_4^+, BC, and OC at 14 sites are displayed in Fig. 3(b)–(f). The concentrations of SO_4^{2-}, BC, and OC are underestimated by about 41%, 55%, and 69%, respectively. The low biases in simulated BC and OC agree closely with those reported by Fu et al. (2012). Nitrate aerosol concentrations are overestimated by 61%, suggesting that NH_3 emissions are overestimated in China (Wang et al., 2013).

The monthly or seasonal mean measured concentrations of O_3 were collected from the literature (Table 4). Most observations were conducted over years of 2001–2009. The scatter plots of simulated versus observed seasonal mean O_3 concentrations are shown in Fig. 4 for the simulations with and without the impacts of aerosols on O_3 (CTRL and NOALL). Consideration of all heterogeneous reactions (hydrolysis of N_2O_5, irreversible absorption of NO_3 and NO_2, and the uptake of HO_2 by aerosols) in the CTRL simulation improves the simulated O_3 concentrations in China; the model overestimates O_3 concentrations with average biases of 9% and 33% in the CTRL and NOALL simulations, respectively.

Comparisons of simulated versus observed concentrations of all aerosol species and O_3 show high correlation coefficients, with values of R^2 ranging from 0.70 to 0.97. These high R^2 values indicate that the model can capture the spatial distributions and seasonal variations of each aerosol species and O_3 despite the biases in simulated concentrations.

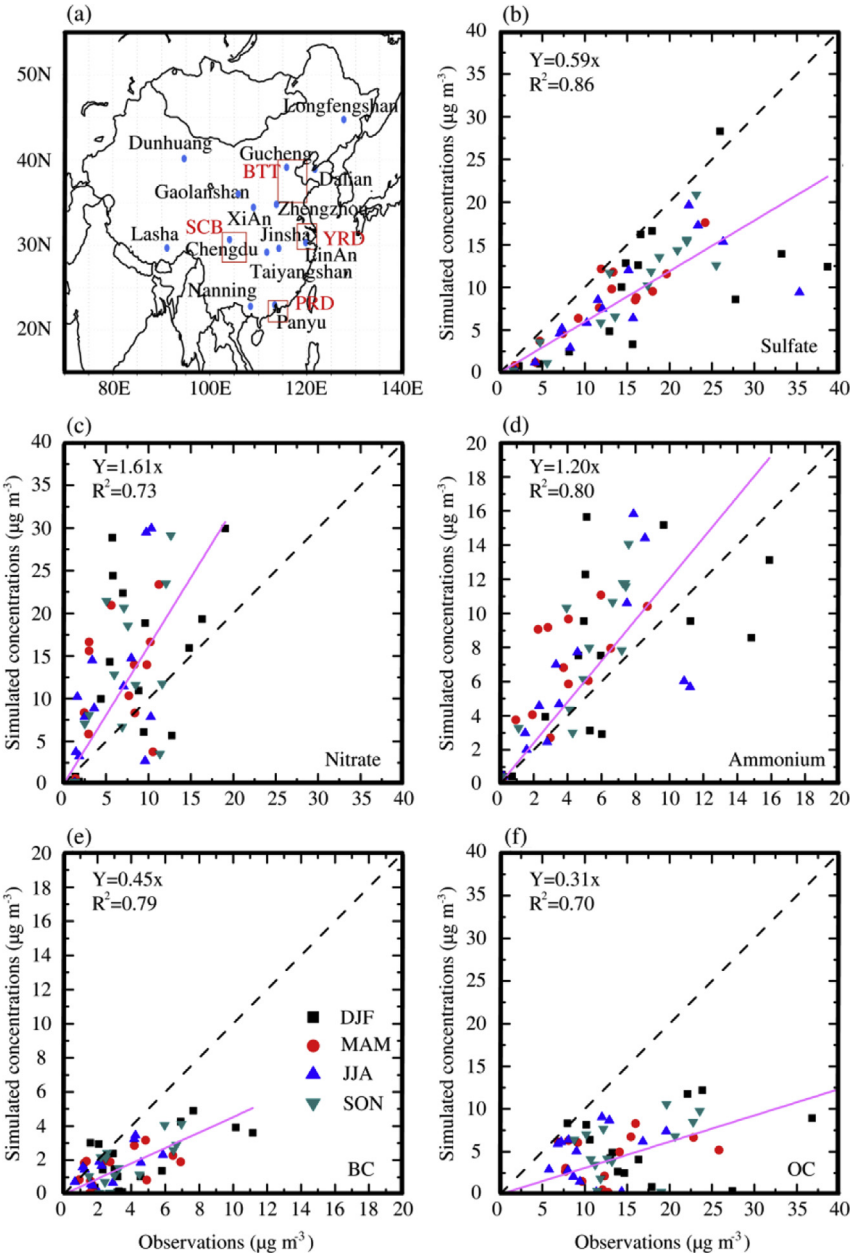

Fig. 3. (a) Locations with measured aerosol concentrations. The 4 polluted regions examined in this study are also shown, including Beijing–Tianjin–Tanggu (BTT, 35°–40°N, 114°–120°E), Yangtze River Delta (YRD, 29.5°–32.5°N, 118°–122°E), Pearl River Delta (PRD, 21°–23.5°N, 112–116°E), and Sichuan Basin (SCB, 28°–31.5°N, 102.5°–107.5°E). Fig. 3b–f show the comparisons of simulated concentrations of sulfate, nitrate, ammonium, BC, and OC aerosols with measured values, respectively. Also shown is the 1:1 line (dashed) and linear fit (solid line and equation). *R* is the correlation coefficient between simulated and measured concentrations.

Table 4
Comparisons of simulated O_3 concentrations with measurements.

Locations	Time periods		O_3 concentrations (ppbv)			
			Observed	GEOS-Chem		
				CTRL	NOALL	
Longfengshan (44.7°N, 127.6°E)	Aug. 1994–Jul. 1995	Spring	37.3 ± 5.89	43.59	54.22	Yan et al. (1997)
		Summer	32.9 ± 7.14	44.70	51.43	
		Fall	39.84 ± 6.76	35.76	42.18	
		Winter	29.1 ± 3.00	31.97	40.89	
Shangdianzi (40.7°N, 117.1°E)	2004–2006	Spring	47.3	45.26	54.70	Lin et al. (2008)
		Summer	42.9	58.38	68.20	
		Fall	43.5	39.49	47.00	
		Winter	36.8	40.02	49.56	
Lin'an (31.3°N, 120.4°E)	Aug. 1994–Jul. 1995	Spring	38.8 ± 8.30	48.40	60.54	Yan et al. (1997)
		Summer	30.6 ± 7.99	51.12	58.72	
		Fall	50.4 ± 10.75	43.89	52.78	
		Winter	36.9 ± 9.08	35.53	44.76	
	Nov. 2003–Nov. 2004	Spring	36.34	48.40	60.54	Yang et al. (2008)
		Summer	37.80	51.12	58.72	
		Fall	31.75	43.89	52.78	
		Winter	23.74	35.53	44.76	
	Dec. 1999		32	33.56	41.86	Yan et al. (2003)
	Jun. 2000		40	54.26	63.18	
	18th Feb.–30th Apr., 2001		34	45.81	58.51	Wang et al. (2004)
Waliguan, Qinghai-Tibetan Plateau (36.3°N, 100.9°E)	Aug. 1994–Jul. 1995	Spring	52.2 ± 4.21	53.42	60.26	Yan et al. (1997)
		Summer	60.9 ± 6.87	55.64	59.86	
		Fall	42.1 ± 4.16	49.65	55.14	
		Winter	42.4 ± 2.73	51.43	59.73	
	20th Apr.–23rd May, 2003		58 ± 9	54.89	60.63	Wang et al. (2006)
	15th Jul.–16th Aug., 2003		54 ± 11	54.18	58.82	
Changshu (30.3°N, 119.4°E)	Jun. 2000		45	55.18	64.07	Yan et al. (2003)
	Dec. 1999		22	32.64	40.34	
Fenghuangshan (40.5°N, 124°E)	16th Feb.–2nd Mar., 2001		30.2	37.83	47.53	Takami et al. (2006)
	13rd Jan.–25th Jan. 2000		32.2	33.36	40.79	
Qingdao (36.5°N, 121°E)	24th Feb.–15th Mar., 2002		26.6	41.41	48.49	
	16th Feb.–28th Feb., 2001		23.5	39.64	46.91	
	15th Jan.–28th Jan., 2000		35.9	34.97	42.43	
Miyun (40.5°N, 116.8°E)	2006	Spring	48.7	43.1	52.02	Wang et al. (2011)
		Summer	57.8	56.4	70.21	
		Fall	39.3	37.8	45.62	
		Winter	27.0	38.5	48.41	
Nanjing (32.1°N, 118.7°E)	Jan. 2000–Feb. 2003	Spring	27.0	48.67	59.41	Tu et al. (2007)
		Summer	22.8	53.19	60.70	
		Fall	18.4	43.08	52.55	
		Winter	14.1	32.75	42.38	
Hong Kong (22.2°N, 114.2°E)	1994–2007	Spring	35.5	43.2	49.80	Wang et al. (2009)
		Summer	19.8	36.1	38.11	
		Fall	42.7	49.1	57.31	
		Winter	37.8	44.1	48.36	
Guangzhou (23.1°N, 113.3°E)	Oct. 2004		29	50.62	63.35	Zhang et al. (2008)
Xinken (22.6°N, 113.6°E)	Oct. 2004		49	54.34	64.25	
PRD region	Oct. 2004		68	57.07	67.20	

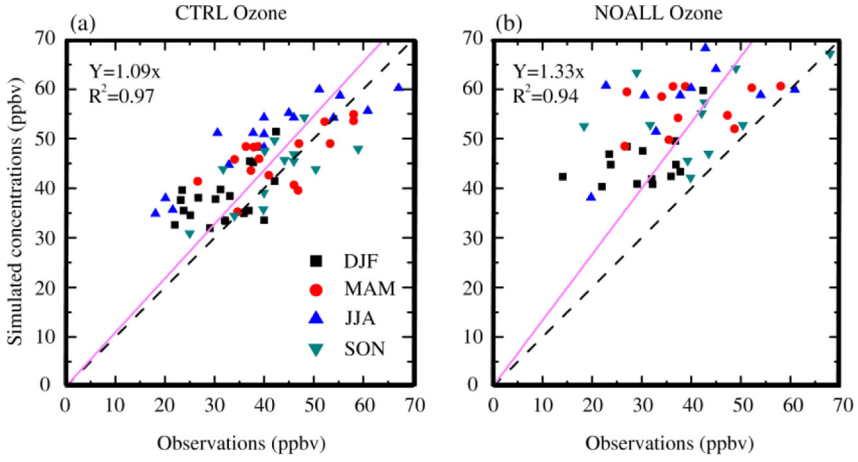

Fig. 4. The comparisons of simulated concentrations of O_3 with measurements for (a) the CTRL run and (b) NOALL simulation.

4. Simulated impacts of aerosols on tropospheric O_3 by heterogeneous reactions

4.1. Impacts on surface-layer concentrations of NO_x, OH, and O_3

4.1.1. NO_x

To understand the impacts of heterogeneous reactions on surface-layer O_3, we examine firstly the impacts of each and all heterogeneous reactions on surface-layer NO_x concentrations. NO_x is defined as $NO + NO_2 + NO_3 + HNO_2$ in the GEOS-Chem simulation. In the presence of all heterogeneous reactions, simulated NO_x concentrations show reductions in all seasons in China (Fig. 5). The simulated reductions are the largest in DJF, with the maximum reductions reaching 12–14 ppbv over Henan and Hubei provinces in central China. The reductions in NO_x are much smaller in other seasons, with maximum reductions of 2–4 ppbv in MAM and JJA and of 4–8 ppbv in SON over the North China Plain.

Both the hydrolysis of N_2O_5 and the absorption of NO_2 and NO_3 are simulated to lead to reductions in NO_x, whereas the uptake of HO_2 is found to lead to small increases in NO_x concentrations (Fig. 5). With the assumed uptake coefficients, the absorption of NO_2 and NO_3 is simulated to be the dominant factor that leads to reductions in NO_x in all seasons; the largest reductions in NO_x are 6–9 ppbv over the North China Plain and in the middle and lower reaches of the Yangtze River in DJF, as a result of the highest concentrations of NO_x in this season and the direct removal of NO_x from the atmosphere, and the reductions in NO_x are in the range of 1–4 ppbv in MAM and JJA and of 2–6 ppbv in SON. Over eastern China, the maximum reductions in NO_x by hydrolysis of N_2O_5 are 1–4 ppbv in DJF and 0.5–2 ppbv in other seasons. The uptake coefficient of N_2O_5 is dependent on temperature and relative humidity, which is calculated to be higher in winter than in summer in the northern mid-latitudes (30–60°N), as reported by Evans and Jacob (2005) using the same $\gamma_{N_2O_5}$ in the GEOS-Chem model. The uptake of HO_2 by aerosols leads to slightly positive changes in NO_x, because the depletion of OH increases the lifetime of NO_x via reduction of the reaction $NO_2 + OH$ (Martin et al., 2003).

In our work the presence of all heterogeneous reactions is simulated to lead to reductions in NO_x by 20–80% in DJF and by 5–30% in JJA over eastern China, which are smaller than the percentage reductions in NO_x reported by Dentener and Crutzen (1993). With larger uptake coefficients ($\gamma_{N_2O_5}$ = 0.1, and γ_{NO_3} = 0.1 on sea salt and 10^{-3} on other aerosols) than those in our study (Table 1), Dentener and Crutzen (1993) found that the heterogeneous reactions of N_2O_5 and NO_3 reduce zonal mean NO_x by 60–80% in winter and by 20–30% in summer in the mid-latitudes of Northern Hemisphere. In the presence of all heterogeneous reactions, NO_x is simulated to decrease by 5–30% in March of year 2005 in our study. However, Martin et al. (2003) found increases in NO_x concentration of 10–30% by aerosol uptakes of HO_2, NO_2, and NO_3 in March of year 1997 by using an earlier version of the GEOS-Chem model. The higher uptake coefficient of γ_{HO_2} of 0.2 in Martin et al. (2003) led to a significant reduction in OH and hence longer lifetime of NO_x.

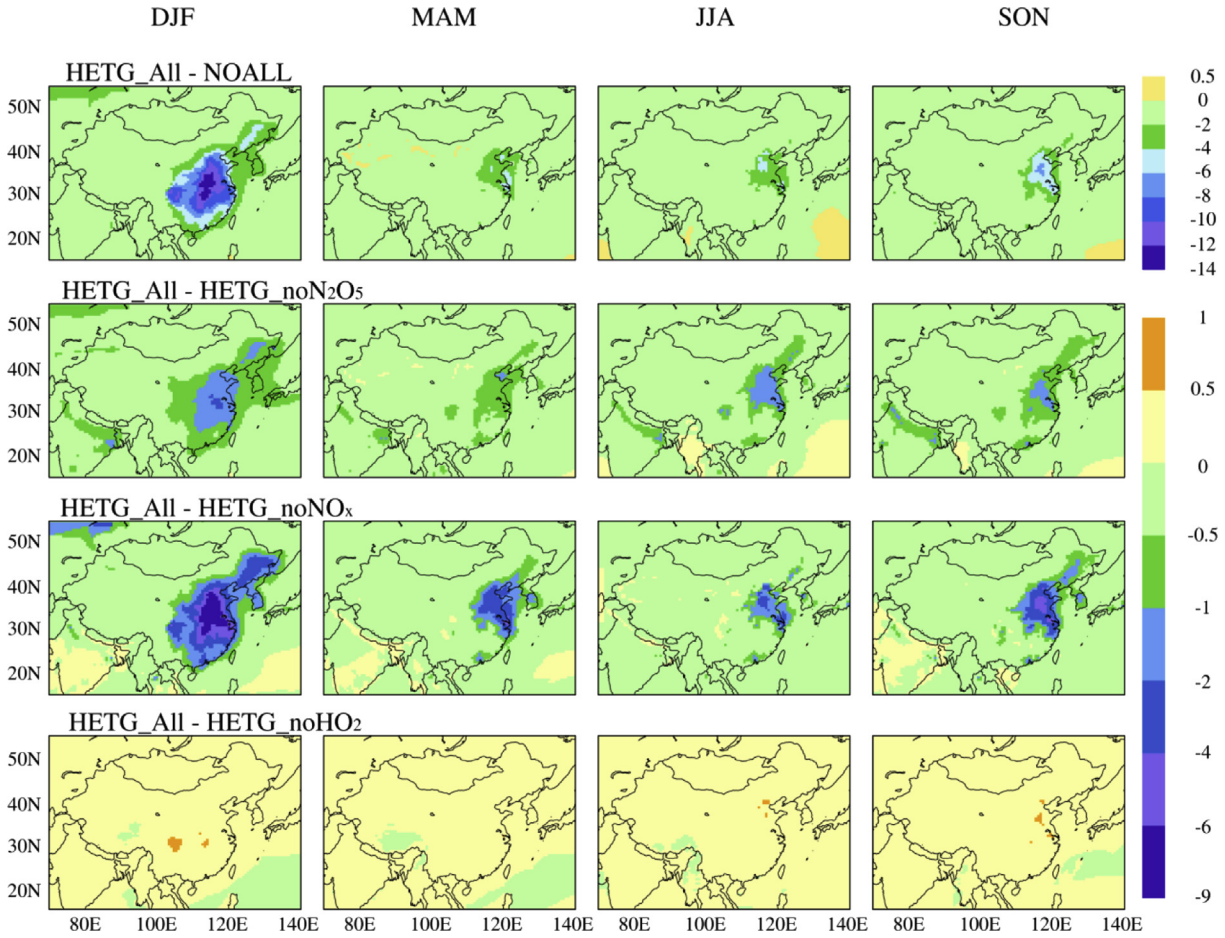

Fig. 5. Simulated impacts of aerosols on seasonal mean surface-layer NO_x concentrations (ppbv) by all heterogeneous reactions (HETG_All−NOALL), the uptake of N_2O_5 (HETG_All−HETG_noN_2O_5), the absorption of NO_2 and NO_3 (HETG_All−HETG_noNO_x), and the uptake of HO_2 (HETG_All−HETG_noHO_2).

4.1.2. OH

The production of OH radical is initiated by photolysis of O_3 (Seinfeld and Pandis, 2006) and the loss of OH in highly polluted regions is mainly through $NO_2 + OH$ (Jacob, 2000). Simulated impacts of heterogeneous reactions on seasonal mean surface-layer OH concentrations are shown in Fig. 6. Compared to the NOALL simulation, the consideration of all heterogeneous reactions (reactions of N_2O_5, NO_2, NO_3, and HO_2 on aerosol surfaces) in HETG_All increases OH concentrations over polluted areas in eastern China and reduces OH concentrations in relatively clean regions such as western China; the simulated changes in surface-layer OH concentrations exhibit the largest increases of 70–90 $\times 10^4$ molecules cm^{-3} in DJF over southeastern China and SCB whereas prevailing decreases of 30–60 $\times 10^4$ molecules cm^{-3} in JJA in a large fraction of eastern China. Pozzoli et al. (2008) reported reductions in surface-layer OH concentrations of 5% and 18% over the northern (25–45°N, 120–155°E) and southern (10–25°N, 110–155°E) TRACE-P regions, respectively, in March of 2001. In this study, changes in OH of +1% and −16% are simulated in March of 2005 (not shown) in these two regions, respectively, with the same $\gamma_{N_2O_5}$, γ_{NO_2}, and γ_{NO_3} as in Pozzoli et al. (2008) but a smaller γ_{HO_2} of about 0.07 than that of 0.2 in Pozzoli et al. (2008).

The hydrolysis of N_2O_5 is simulated to increase surface-layer OH concentrations by up to 20 $\times 10^4$ molecules cm^{-3} in a large fraction of eastern China in DJF and in polluted North China Plain and Yangtze River Delta in other seasons, which can be explained by reductions in NO_x in these VOC-limited regions (Fig. 5), leading to increases in O_3 and hence increases in OH. On the contrary, the reductions in NO_x by hydrolysis of N_2O_5 are simulated to lead to decreases in OH in NO_x-limited suburban regions in eastern China.

The absorption of NO_2 and NO_3 is simulated to be the dominant factor that leads to increases in OH in all seasons, as a result of the less removal of OH by the reaction of $NO_2 + OH$ and the increases in OH through photolysis of HONO produced by absorption of NO_2 (Table 1). The large increases in OH of 50–70 $\times 10^4$ molecules cm^{-3} are found over eastern China in DJF and SON because of the largest concentrations of aerosols (Fig. 2) and the largest reductions in NO_x by absorption of NO_2 and NO_3 (Fig. 5). The maximum increases in OH over the YRD are about 50–60 $\times 10^4$ molecules cm^{-3} in MAM and JJA.

The reaction of HO_2 is simulated to lead to negative changes in OH concentrations via removal of HO_x from the atmosphere, with maximum reductions in OH of 50–80 $\times 10^4$ molecules cm^{-3} in JJA over the North China Plain (as a result of the relatively high aerosol concentrations and the most sufficient OH in summer) and of 30–50 $\times 10^4$ molecules cm^{-3} over southeastern China in other seasons.

4.1.3. Ozone

Simulated impacts of each and all heterogeneous reactions on seasonal mean surface-layer O_3 concentrations are shown in Fig. 7. In DJF, the presence of all heterogeneous reactions is simulated to reduce O_3 concentrations by 8–12 ppbv in northern China and by 4–8 ppbv over the Tibet Plateau, as a result of the dominant impact of hydrolysis of N_2O_5. On the contrary, DJF O_3 concentrations in

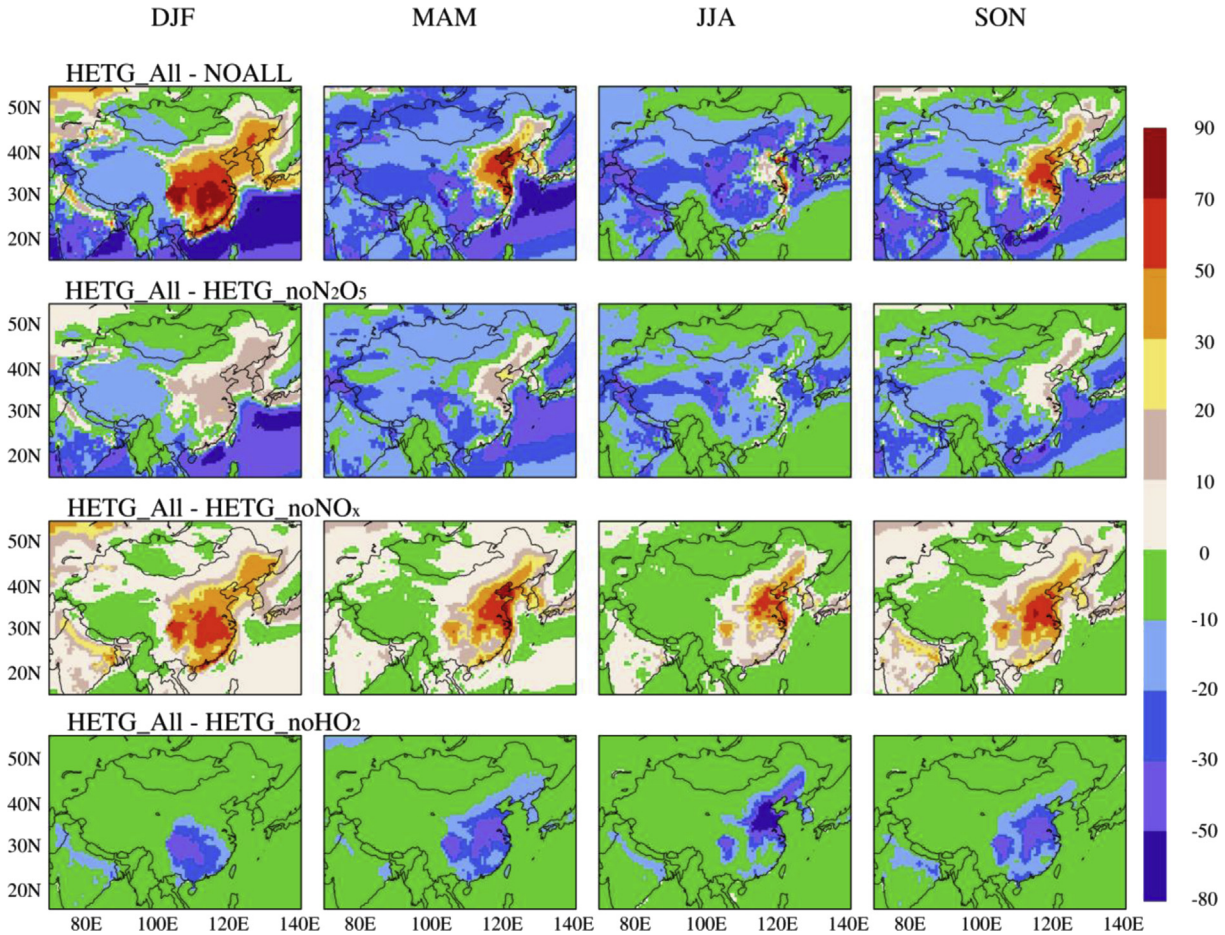

Fig. 6. Simulated impacts of aerosols on seasonal mean surface-layer OH concentrations (10^4 molecules cm^{-3}) by all heterogeneous reactions (HETG_All−NOALL), the uptake of N_2O_5 (HETG_All−HETG_noN_2O_5), the absorption of NO_2 and NO_3 (HETG_All−HETG_noNO_x), and the uptake of HO_2 (HETG_All−HETG_noHO_2).

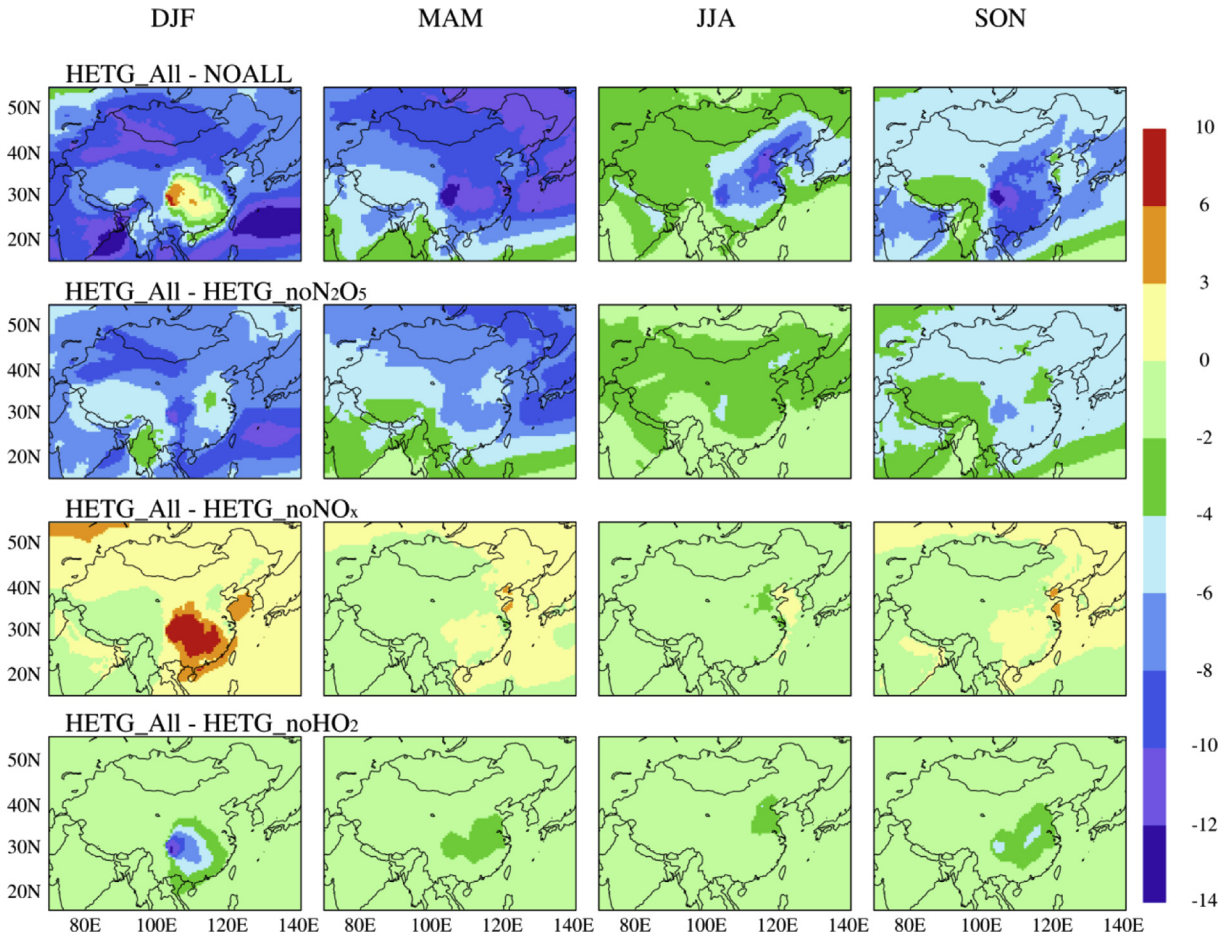

Fig. 7. Simulated impacts of aerosols on seasonal mean surface-layer O_3 concentrations (ppbv) by all heterogeneous reactions (HETG_All−NOALL), the uptake of N_2O_5 (HETG_All−HETG_noN_2O_5), the absorption of NO_2 and NO_3 (HETG_All−HETG_noNO_x), and the uptake of HO_2 (HETG_All−HETG_noHO_2).

southern China are simulated to increase as a result of the dominant impact of absorption of NO_x by aerosols, with the maximum increases in O_3 reaching 3–6 ppbv in SCB. Concentrations of O_3 in MAM, JJA, and SON all show larger reductions in eastern China than in western China; simulated reductions in eastern China are 6–14 ppbv in MAM and SON and 4–12 ppbv in JJA. On an annual mean basis, the presence of all heterogeneous reactions is simulated to lead to reductions in O_3 by 10–18% over eastern China. It should be noted that the locations of maximum reductions in O_3 are not necessarily the places of maximum $PM_{2.5}$ concentrations, which will be discussed further below.

With the assumed uptake coefficients in this study, the hydrolysis of N_2O_5 is simulated to be the dominant factor that leads to reductions in O_3 in all seasons. Although the uptake of HO_2 is also simulated to reduce O_3 concentrations, the magnitude of reductions is smaller (Fig. 7). With the absorption of HO_2 by aerosols alone, our simulated reductions in annual mean concentration of O_3 are 1–6 ppbv, which are smaller than the annual mean reductions of 11–15 ppbv found over eastern China in Mao et al. (2013), since Mao et al. (2013) used an updated large γHO_2 of 1.0 in the GEOS-Chem model. It is interesting to note that the uptake of N_2O_5 has large impacts nationwide whereas the impacts of the absorption of NO_x and HO_2 uptake are mainly found over the polluted eastern China. The assumed uptake coefficient of N_2O_5 reaction is about 0.02–0.03 from surface to 600 hPa altitude in the middle latitudes of Northern Hemisphere (Evans and Jacob, 2005) and N_2O_5 exists in the lower to middle troposphere (Bell et al., 2005), which lead to reductions in O_3 in China by reducing O_3 in the upstream areas such as Europe. However, the absorption of NO_2 and NO_3 is less important in the lower to middle troposphere because of the smaller uptake coefficient (Table 1). Although γ_{HO_2} is about 0.01–0.05 below 4 km in the middle latitudes of North Hemisphere (Thornton et al., 2008), reductions in O_3 are mainly at the surface because O_3 production is sensitive to changes in HO_x in VOC-limited areas (Seinfeld and Pandis, 2006).

We also examine the net chemical production of O_3 (chemical production − chemical loss) in the lowest 2 km of the model layers in the presence of each and all heterogeneous reactions (Fig. 8). Compared to the NOALL simulation, heterogeneous reactions in HETG_All are simulated to lead to negative net O_3 production in MAM, JJA, and SON in China except for the positive net O_3 production found in the VOC-limited BTT in MAM and SON. The negative net O_3 production results from the decreases in NO_x (Fig. 5), contributing to the large reductions in O_3 in the presence of all heterogeneous reactions (Fig. 7). In DJF, however, positive net O_3 production is simulated in eastern China and SCB as a result of the reactions of NO_2 and NO_3, because eastern China and SCB are generally VOC-limited in winter (Liu et al., 2010). The uptake of NO_2 and NO_3 by aerosols reduces NO_x but increases OH (Figs. 5 and 6), leading to increases in O_3 production in the VOC-limited regions via enhanced HO_2 yield and accelerated conversion of NO–NO_2 (An et al., 2013). Both the hydrolysis of N_2O_5 and the uptake of HO_2 lead to generally negative net O_3 production in eastern China throughout the year, consistent with the changes in NO_x (Fig. 5) and

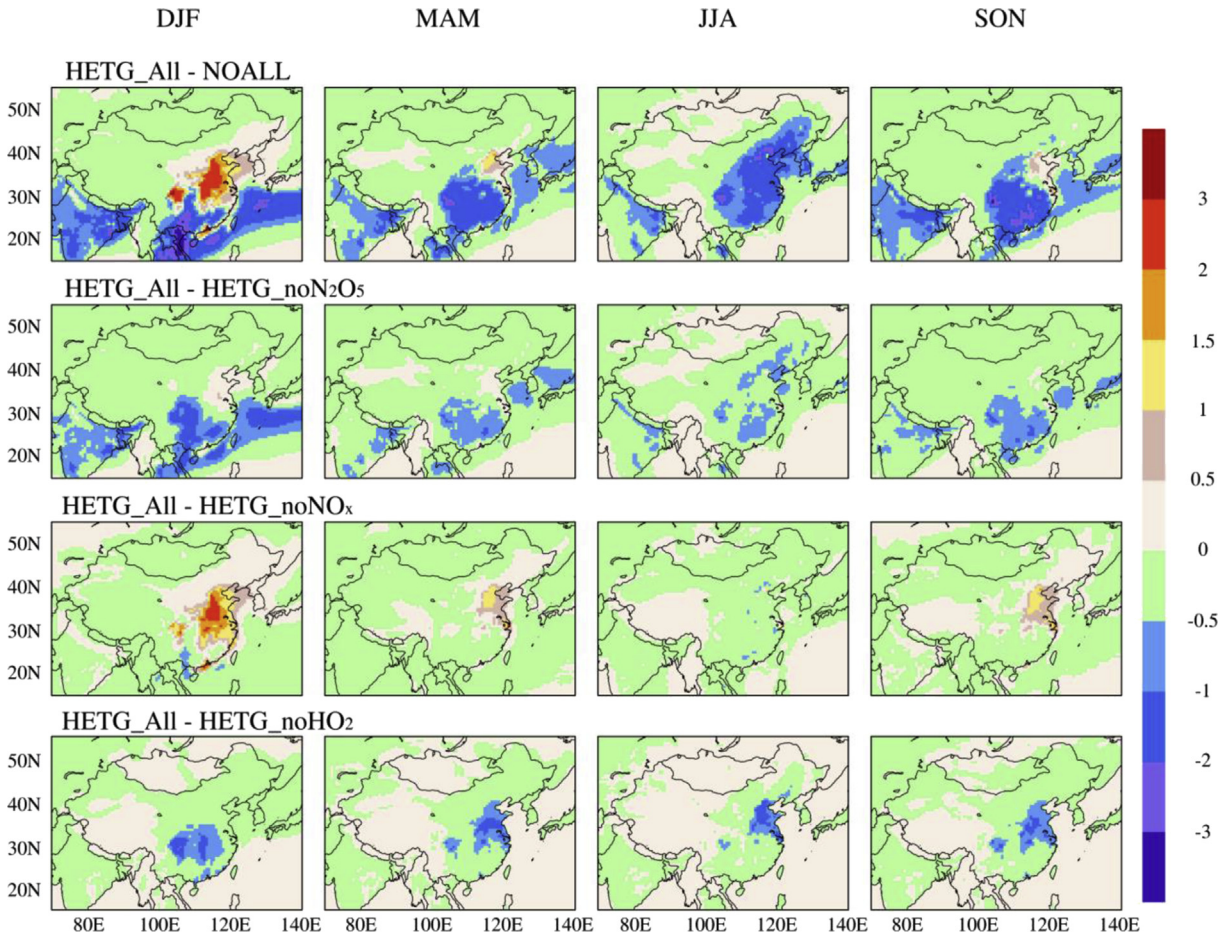

Fig. 8. Simulated impacts of aerosols on seasonal mean net O_3 production (prodution−loss, sum from 1000 to 800 hPa, unit: kg s^{-1} $grid^{-1}$) by all heterogeneous reactions (HETG_All−NOALL), the uptake of N_2O_5 (HETG_All−HETG_noN_2O_5), the absorption of NO_2 and NO_3 (HETG_All−HETG_noNO_x), and the uptake of HO_2 (HETG_All−HETG_noHO_2).

the reductions in OH (Fig. 6). Note that the net chemical production is only one of the factors that contribute to the changes in O_3 in Fig. 7; the changes in O_3 in a specific location are coupled with the transport of O_3 from surrounding areas.

4.1.4. *Impacts on monthly O_3 concentrations over the four polluted regions*

The impacts of heterogeneous reactions on monthly O_3 concentrations over the four polluted regions BTT, YRD, PRD, and SCB are shown in Fig. 9. In BTT, in the presence of all heterogeneous reactions, large reductions in O_3 of 7.7–10.3 ppbv (or 13.5–21.6% relative to the values simulated in NOALL) are simulated in January–September and lower reductions of 4.9–7.1 ppbv (or 12.3–17.2%) are found in October–December. The hydrolysis of N_2O_5 has the largest impact on O_3 concentrations in BBT, followed by the uptake of HO_2 and the absorption of NO_x. In YRD, PRD, and SCB, the impacts of heterogeneous reactions are generally the smallest in summer, since aerosol concentrations are the lowest in this season (Fig. 9) as a result of the removal of aerosols by precipitation associated with the summer monsoon. The largest reductions of O_3 in YRD are simulated to be 11.2 ppbv (or 19.9%) in MAM, and those in PRD are 10.1 ppbv (or 17.1%) in MAM. The impacts of all heterogeneous reactions are the most significant in SCB, with reductions in O_3 exceeding 14 ppbv (or 21.5%) in March and November.

The impact of aerosols on O_3 concentration by heterogeneous reactions can be characterized by the ratio of change in O_3 concentration ($\Delta[O_3]$) to local $PM_{2.5}$ level ($[PM_{2.5}]$), ROP = $\Delta[O_3]/[PM_{2.5}]$. The annual mean values of *ROP* are calculated to be −0.14, −0.17, −0.27, and −0.16 ppbv $(\mu g\ m^{-3})^{-1}$ over BTT, YRD, PRD, and SCB, respectively. Values of ROP show relatively small monthly variations in BTT and YRD; ROP varies between −0.07 and −0.2 ppbv $(\mu g\ m^{-3})^{-1}$ in BTT and between −0.11 and −0.23 ppbv $(\mu g\ m^{-3})^{-1}$ in YRD. Values of ROP in PRD and SCB exhibit large monthly variations and two negative maxima; the largest negative values of ROP are −0.51 ppbv $(\mu g\ m^{-3})^{-1}$ in March and −0.36 ppbv $(\mu g\ m^{-3})^{-1}$ in November in PRD and are −0.32 ppbv $(\mu g\ m^{-3})^{-1}$ in March and −0.25 ppbv $(\mu g\ m^{-3})^{-1}$ in October in SCB. Per unit mass of aerosols may lead to different changes in O_3 concentration in different polluted regions in China, since the uptake coefficients are dependent on local chemical composition of aerosols, relative humidity, temperature, and the concentrations of O_3 also depend on local chemical (e.g., NO_x to VOC ratio) and meteorological conditions.

5. Simulated impacts of aerosols on surface-layer O_3 by altering photolysis rates

5.1. *Simulated aerosol optical depths (AODs)*

Fig. 10 shows the simulated seasonal mean AODs in the CTRL simulation. Accounting for sulfate, nitrate, ammonium, BC, and OC aerosols, simulated seasonal mean AODs are in the ranges of 0.4–0.7 and 0.3–0.5 over YRD and PRD, respectively. In BBT, while AODs

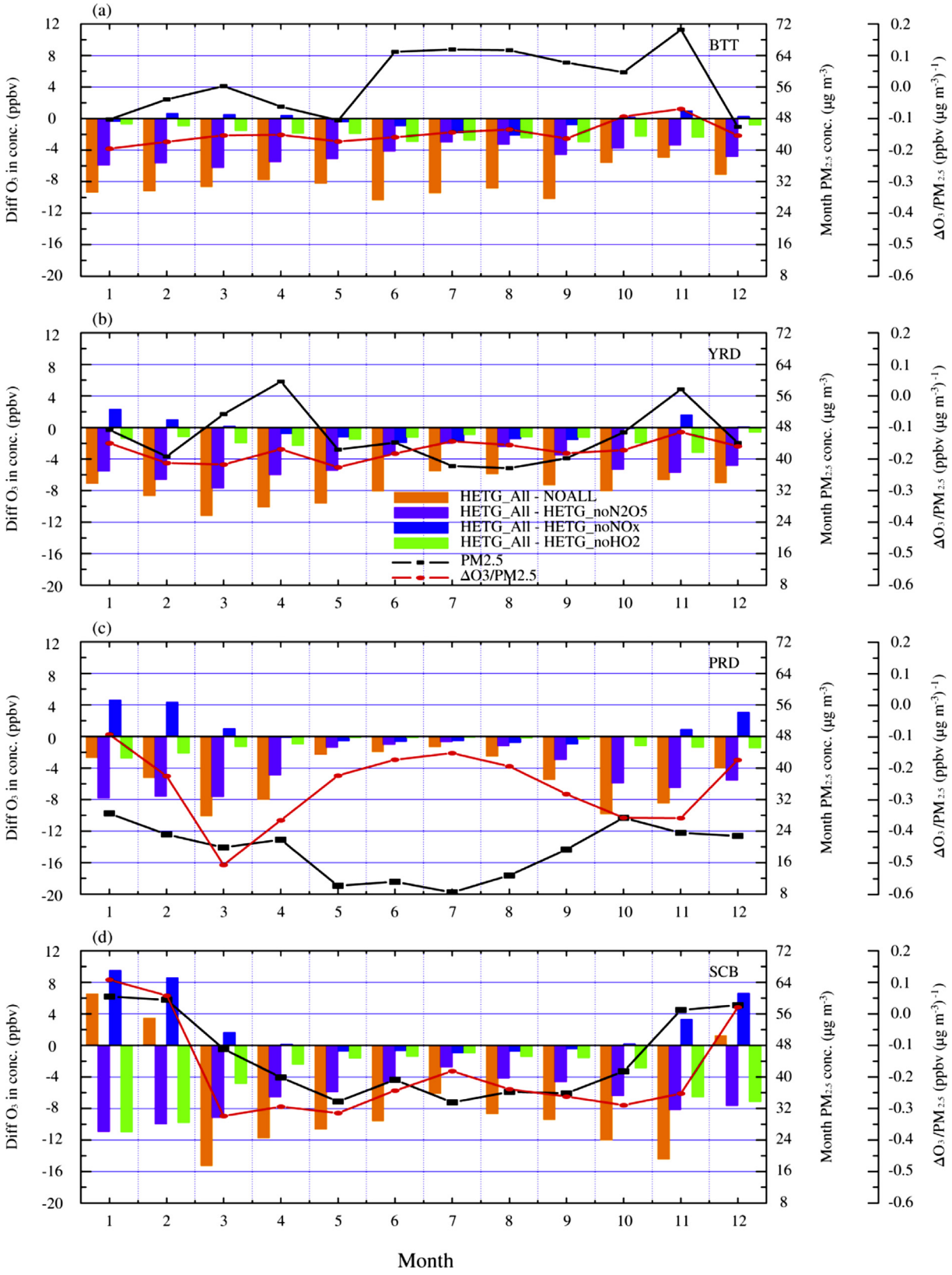

Fig. 9. Simulated monthly impacts of each and all heterogeneous reactions on surface-layer O_3 concentrations (ppbv, left axis) over polluted regions of (a) BTT, (b) YRD, (c) PRD and (d) SCB. Black line represents simulated monthly variations in $PM_{2.5}$ concentrations (μg m^{-3}, first right axis) and red line represents the ratio of change in O_3 to concentration of $PM_{2.5}$ aerosol (*ROP* as defined in the text, ppbv (μg m^{-3})$^{-1}$, second right axis) for each region. See Fig. 3a for definitions of regions of BTT, YRD, PRD, and SCB. (For interpretation of the references to color in this figure legend, the reader is referred to the web version of this article.)

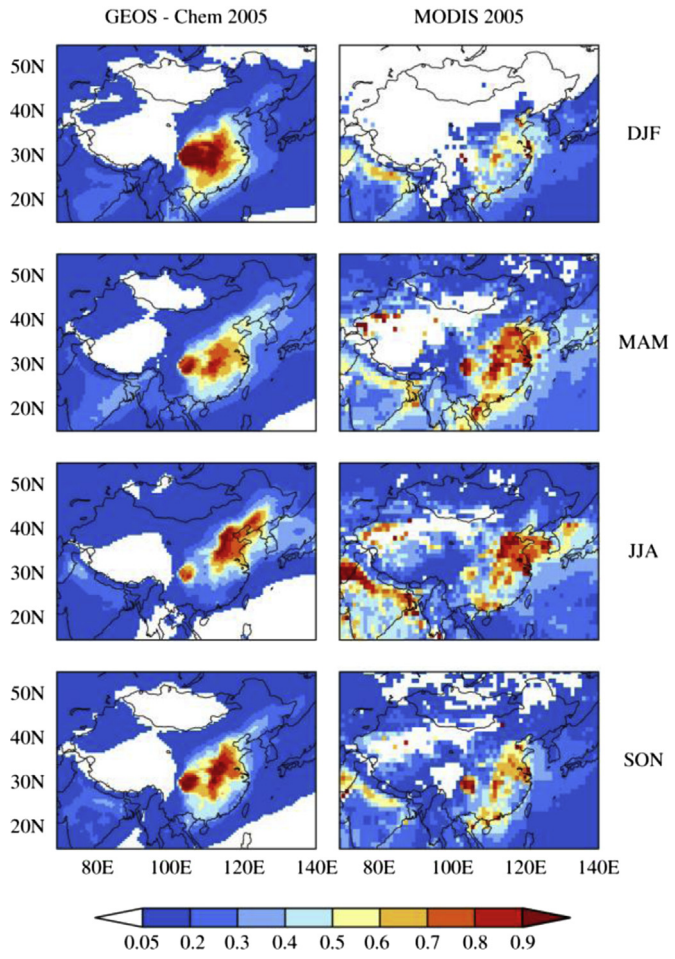

Fig. 10. Comparisons of simulated seasonal mean aerosol optical depth (AOD) (left column) with the MODIS AOD (right column) for year of 2005.

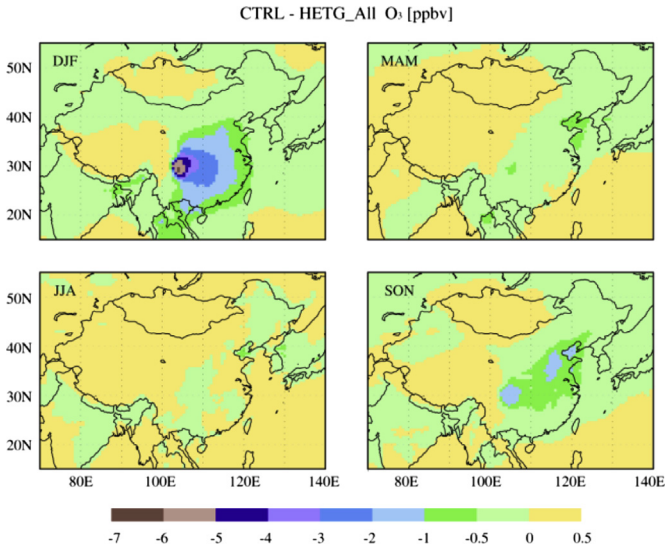

Fig. 11. Simulated changes in seasonal mean surface-layer O_3 concentrations (ppbv) through aerosol effect on photolysis rates (CTRL–HETG_All).

are 0.4–0.7 in DJF, MAM, and SON, AODs are 0.7–1.0 in JJA as a result of large aerosol concentrations (Fig. 2) and high relative humidity in this season. Over SCB, seasonal mean AODs are 0.5–0.8 in MAM and JJA, 0.7–1.0 in SON, and 0.9–1.2 in DJF. The simulated seasonal distributions of AODs agree well with those retrieved from the Moderate Resolution Imaging Spectroradiometer (MODIS) (Fig. 10), but the model overestimates AODs in DJF and underestimates AODs in PRD in all seasons. The high biases of AODs in DJF can be explained by the overestimates of nitrate aerosol (Fig. 3) in that region.

5.2. *Impacts on surface-layer O_3*

The impacts of aerosols on surface-layer O_3 concentrations by altering photolysis rates are obtained by examining the differences in O_3 between the CTRL and HETG_All simulations (CTRL–HETG_All) (Fig. 11). With aerosols, annual mean photolysis rates, $J(O_3 \rightarrow O(^1D))$ and $J(NO_2)$, are simulated to be reduced by 6–18% in polluted eastern China, leading to reductions in O_3 of up to 0.5 ppbv in those regions in MAM and JJA. The reductions in O_3 in SON are 0.5–2 ppbv in BTT and 1–2 ppbv in SCB, which are much smaller than the impacts by heterogeneous reactions. The largest reductions of 3–6 ppbv in O_3 are simulated in SCB in DJF, which can mainly be attributed to the high biases of simulated AOD. Our simulated small changes in O_3 by aerosol-induced changes in photolysis rates agree with previous studies by Tie et al. (2005) and

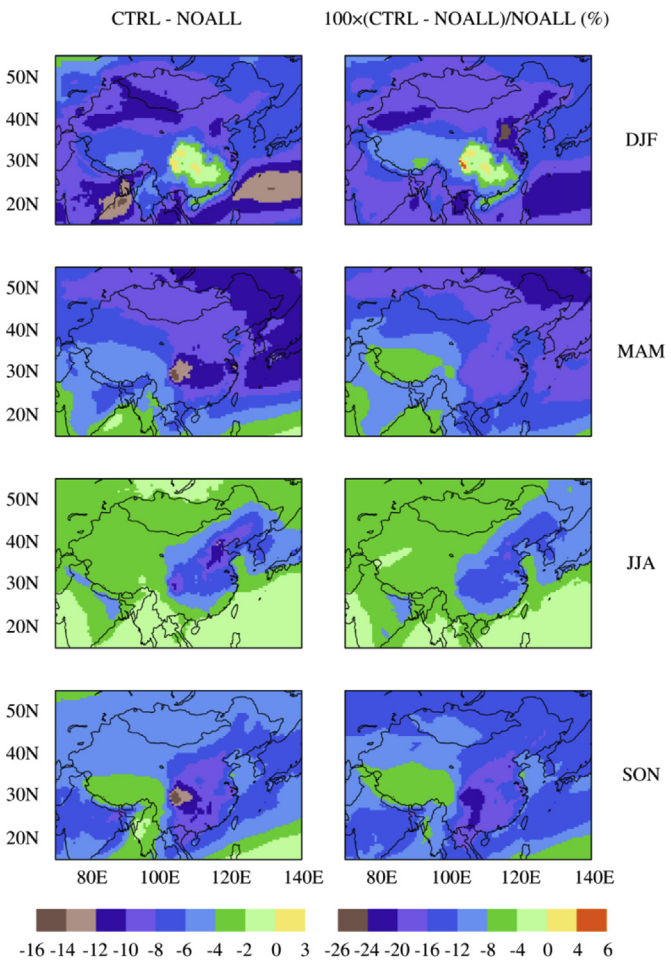

Fig. 12. Simulated impacts of aerosols on seasonal mean surface-layer O_3 concentrations with all heterogeneous reactions and changes in photolysis rates (CTRL–NOALL). Left column shows changes in ppbv and right column shows percentages changes in CTRL simulation relative to NOALL.

Real and Sartelet (2011), who reported less than 4% changes in O_3 concentrations by aerosol radiative effect.

6. Combined impacts of aerosols on O_3 by heterogeneous reactions and changes in photolysis rates

Fig. 12 shows the net impacts on O_3 concentration by aerosols through both heterogeneous reactions and changes in photolysis rates. The reductions in O_3 are simulated all over China in all seasons, except that small increases in O_3 of 0–3 ppbv are found over SCB in DJF. Relative to NOALL, concentrations of O_3 in CTRL are simulated to be reduced by 8–24% north of 30°N in DJF and by 12–20% in a large fraction of China in MAM. The similar percentage reductions in O_3 are also found in JJA and SON, but the reductions in these two seasons occur mainly over the polluted areas.

7. Uncertainties with model results

The results presented in previous sections indicate that heterogeneous reactions have large impacts on surface-layer O_3 in China. These results rely on the assumed uptake coefficients, some of which have large uncertainties. For example, Macintyre and Evans (2010) showed high sensitivity of O_3 to value of $\gamma_{N_2O_5}$ between 0.001 and 0.02; O_3 burden over 30–90°N is simulated to increase by 7% as $\gamma_{N_2O_5}$ is varied from 0.02 to 0.001. Furthermore, we follow the study of Thornton et al. (2008) to assume γ_{HO_2} to be calculated as a function of temperature, relative humidity, and particle size for all aerosol species (Section 2.2) except that a value of 0.07 is specified for sulfate/nitrate/ammonium aerosols in the continental boundary layer. As a result, the calculated γ_{HO_2} is in the range of 0.005–0.05 over eastern China. Recent study of Mao et al. (2013) suggested a new γ_{HO_2} of 1.0 to produce H_2O in the presence of dissolved Cu and Fe through reactions of $HO_2 + HO_2 \rightarrow H_2O_2 + O_2$, $HO_2 + H_2O_2 \rightarrow OH + O_2 + H_2O$, and $HO_2 + OH \rightarrow O_2 + H_2O$ instead of the uptake of HO_2 to form H_2O_2 listed in Table 1. With the uptake of HO_2 by aerosols alone, Mao et al. (2013) simulated an annual mean reductions in O_3 by 11–15 ppbv over eastern China in 2005 (east of 100°E), which are much larger than the reductions of 1–5 ppbv by the uptake of HO_2 in our study. We also note that in our simulation of the impacts of aerosols on gas-phase photolysis rates, aerosol species are treated as an external mixture in the calculation of aerosol optical properties. As shown by Liao et al. (1999), an external mixture of BC with scattering aerosols leads to smaller reductions in photolysis rates than an internal mixture.

Uncertainties in model results also arise from the simulated aerosol concentrations. In our study, sulfate concentrations are underestimated by 31% and nitrate concentrations are

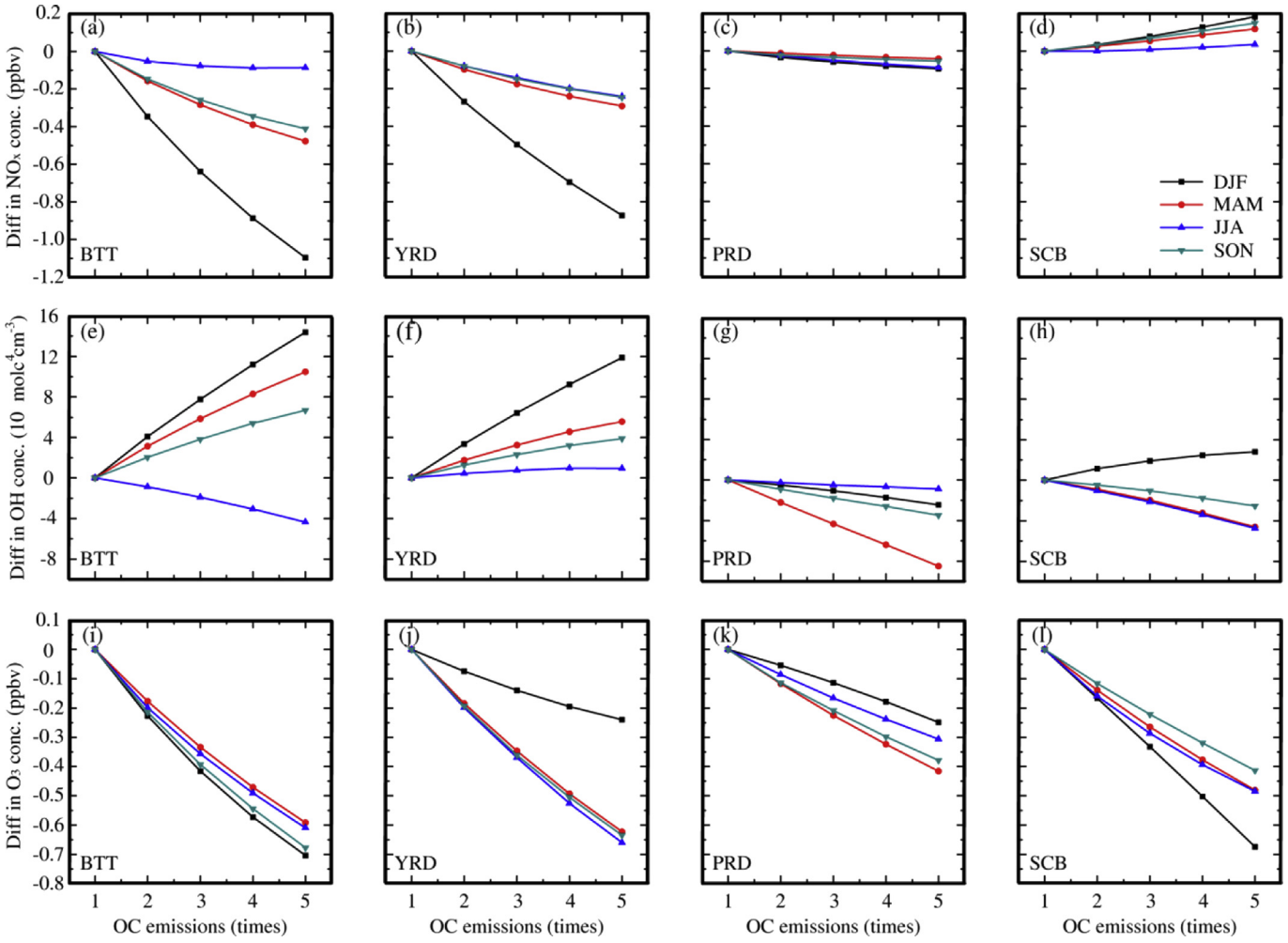

Fig. 13. Simulated impacts of aerosols on seasonal mean surface-layer concentrations of NO_x (a–d), OH (e–h), and O_3 concentrations (i–l) as OC emissions are increased from default values (represented by 1 in horizontal axis) to 2–5 times the default values (represented by numbers 2–5 in horizontal axis) for BTT, YRD, PRD, and SCB regions. Units are ppbv for NO_x (top row), 10^4 molecules cm^{-3} for OH (middle row), and ppbv for O_3 (bottom row). See Fig. 3a for definitions of regions of BTT, YRD, PRD, and SCB.

overestimated by 61% (Section 3.3), which indicate that the total impact on O_3 concentrations by secondary inorganic aerosols are probably reasonable because of the assumed same uptake coefficients on these two aerosols and the same optical properties (refractive index) of sulfate and nitrate used in the calculation of photolysis rates. Considering that concentrations of OC are underestimated by about 69% in this work (Fig. 3), we perform sensitivity simulations to see how the impacts of aerosols on O_3 may change with increased OC emissions (EMIS–CTRL). As OC emissions are increased from default values to 5 times the default values (emissions of other aerosols or aerosol precursors are kept unchanged), O_3 concentrations are simulated to decrease by less than 0.8 ppbv over all the four polluted regions. This can be explained by that N_2O_5 is already depleted in the CTRL simulation (not shown) and hence increases in OC in the atmosphere in simulation EMIS cannot lead to large reductions in NO_x and O_3 (Fig. 13). Moreover, the uptake coefficient of HO_2 on OC (about 0.02 in Thornton et al., 2008) is smaller than that on sulfate/nitrate/ammonium aerosols, which also causes small changes in O_3.

Note that the heterogeneous reactions on mineral dust aerosols can influence O_3 concentrations in China (Tang et al., 2004; Liao and Seinfeld, 2005; Tie et al., 2005; Pozzoli et al., 2008; Fairlie et al., 2010), especially in spring when dust concentrations are the highest. For example, Tang et al. (2004) simulated decreases in O_3 concentrations by 3–7% over eastern China during a dust event in April 4–14, 2001, and Pozzoli et al. (2008) found that simulated surface-layer O_3 concentrations can be reduced by 2–3% by heterogeneous reactions on mineral dust aerosol over the TRACE-P region in March of 2001.

8. Conclusions

We use the global chemical transport model GEOS-Chem to quantify the impacts of aerosols (SO_4^{2-}, NO_3^-, NH_4^+, BC, and OC) on tropospheric O_3 concentrations over China through heterogeneous reactions (including hydrolysis of N_2O_5, irreversible absorption of NO_3 and NO_2 on wet aerosols, and the uptake of HO_2 by aerosols) and changes in photolysis rates. Consideration of these impacts of aerosols improves the simulated O_3 concentrations in China; the averaged biases in simulated O_3 in China are +9% and +33% with and without the impacts of aerosols, respectively.

The impacts of heterogeneous reactions on O_3 are simulated to exhibit large spatial and temporal variations. In DJF, the presence of all heterogeneous reactions is simulated to reduce O_3 concentrations by 8–12 ppbv in northern China but to increase O_3 concentrations by 3–6 ppbv in southern China. Reductions in O_3 concentrations are found to occur all over China in other seasons, with reductions exceeding 6 ppbv in a large fraction of China in MAM and over eastern China in JJA and SON. On an annual mean basis, the heterogeneous reactions are simulated to lead to reductions in O_3 in eastern China by 10–18%.

Different heterogeneous reactions play different roles in influencing O_3 concentrations in China. Both the hydrolysis of N_2O_5 and the uptake of HO_2 are simulated to lead to reductions in O_3. With the assumed uptake coefficients in this work, the hydrolysis of N_2O_5 has a dominant role in reducing O_3 concentrations in China. On the contrary, the absorption of NO_2 and NO_3 is found to lead to increases O_3 concentrations by 3–10 ppbv in DJF and by up to 3 ppbv in other seasons. The uptake of NO_2 and NO_3 by aerosols reduces NO_x but increases OH, leading to increases in O_3 production in the VOC-limited regions via enhanced HO_2 yield and accelerated conversion of NO to NO_2. Our model results also show that the uptake of N_2O_5 has large impacts on O_3 nationwide whereas the impacts of the absorption of NO_x and HO_2 uptake are mainly found over the polluted eastern China. The hydrolysis of N_2O_5 leads to reductions in O_3 in China by reducing O_3 in the upstream areas in the middle latitudes in the Northern Hemisphere.

The impact of aerosols on O_3 concentration through heterogeneous reactions is characterized in this work by the ratio of change in O_3 concentration to local $PM_{2.5}$ level (ROP = $\Delta[O_3]/[PM_{2.5}]$). The locations of maximum reductions in O_3 are not necessarily the places of maximum aerosol concentrations; the annual mean values of ROP are calculated to be −0.14, −0.17, −0.27, and −0.16 ppbv $(\mu g\ m^{-3})^{-1}$ over the heavily polluted regions of Beijing–Tianjin–Tanggu, Yangtze River Delta, Pearl River Delta, and Sichuan Basin, respectively. The impacts of aerosols on O_3 through altering photolysis rates are simulated to be much smaller than the effects of heterogeneous reactions in China.

Acknowledgments

This work was supported by the Chinese Academy of Sciences Strategic Priority Research Program Grant No. XDA05100503, the National Natural Science Foundation of China under grant 41021004, as well as the China Meteorological Administration special funding in atmospheric science GYHY200906020.

References

An, J.L., Li, Y., Chen, Y., Li, J., Qu, Y., Tang, Y.J., 2013. Enhancements of major aerosol components due to additional HONO sources in the North China Plain and implications for visibility and haze. Adv. Atmos. Sci. 30, 57–66.

Andreae, M.O., Schmid, O., Yang, H., Chand, D., Yu, J.Z., Zeng, L.M., Zhang, Y.H., 2008. Optical properties and chemical composition of the atmospheric aerosol in urban Guangzhou, China. Atmos. Environ. 42, 6335–6350.

Alexander, B., Park, R.J., Jacob, D.J., Li, Q.B., Yantosca, R.M., Savarino, J., Lee, C.C.W., Thiemens, M.H., 2005. Sulfate formation in sea-salt aerosols: constraints from oxygen isotopes. J. Geophys. Res. 110, D10307. http://dx.doi.org/10.1029/2004JD005659.

Bell, N., Koch, D., Shindell, D.T., 2005. Impacts of chemistry-aerosol coupling on tropospheric ozone and sulfate simulations in a general circulation model. J. Geophys. Res. 110, D14305. http://dx.doi.org/10.1029/2004JD005538.

Bey, I., Jacob, D.J., Yantosca, R.M., Logan, J.A., Field, B., Fiore, A.M., Li, Q., Liu, H., Mickley, L.J., Schultz, M., 2001. Global modeling of tropospheric chemistry with assimilated meteorology: model description and evaluation. J. Geophys. Res. 106, 23,073–23,096.

Bian, H.S., Prather, M.J., 2002. Fast-J2: accurate simulation of stratospheric photolysis in global chemical models. J. Atmos. Chem. 41, 281–296.

Cao, J.J., Lee, S.C., Chow, J.C., Watson, J.G., Ho, K.F., Zhang, R.J., Jin, Z.D., Shen, Z.X., Chen, G.C., Kang, Y.M., Zou, S.C., Zhang, L.Z., Qi, S.H., Dai, M.H., Cheng, Y., Hu, K., 2007. Spatial and seasonal distributions of carbonaceous aerosols over China. J. Geophys. Res. 112, D22S11. http://dx.doi.org/10.1029/2006JD008205.

Chen, D., Wang, Y.X., McElroy, M.B., He, K., Yantosca, R.M., Le Sager, P., 2009. Regional CO pollution in China simulated by the high-resolution nested-grid GEOS-Chem model. Atmos. Chem. Phys. 9, 3825–3839.

DeMore, W.B., Sander, S.P., Golden, D.M., Hampson, R.F., Kurylo, M.J., Howard, C.J., Ravishankara, A.R., Kolb, C.E., Molina, M.J., 1997. Chemical Kinetics and Photochemical Data for Use in Stratospheric Modeling. JPL Publication 97–4, Pasadena, California.

Dentener, F.J., Crutzen, P.J., 1993. Reaction of N_2O_5 on tropospheric aerosols: impact on the global distributions of NO_x, O_3, and OH. J. Geophys. Res. 98, 7149–7163.

Drury, E., Jacob, D.J., Spurr, R.J.D., Wang, J., Shinozuka, Y., Anderson, B.E., Clark, A.D., Dibb, J., McNaughton, C., Weber, R., 2010. Synthesis of satellite (MODIS), aircraft (ICARTT), and surface (IMPROVE, EAP-AQS, AERONET) aerosol observations over North America to improve MODIS aerosol retrievals and constrain surface aerosol concentrations and sources. J. Geophys. Res. 115, D14204. http://dx.doi.org/10.1029/2009JD012629.

Evans, M.J., Jacob, D.J., 2005. Impact of new laboratory studies of N_2O_5 hydrolysis on global model budgets of tropospheric nitrogen oxides, ozone, and OH. Geophys. Res. Lett. 32, L09813. http://dx.doi.org/10.1029/2005GL022469.

Exner, M., Herrmann, H., Zellner, R., 1992. Laser-based studies of reactions of the nitrate radical in aqueous solution. Ber. Bunsenges. Phys. Chem. 96, 470–477.

Exner, M., Herrmann, H., Zellner, R., 1994. Rate constants for the reactions of the NO_3 radical with $HCOOH/HCOO^-$ and CH_3COOH/CH_3COO^- in aqueous solution between 278 and 328 K. J. Atmos. Chem. 18, 359–378.

Fairlie, T.D., Jacob, D.J., Dibb, J.E., Alexander, B., Avery, M.A., van Donkelaar, A., Zhang, L., 2010. Impact of mineral dust on nitrate, sulfate, and ozone in transpacific Asian pollution plumes. Atmos. Chem. Phys. 10, 3999–4012.

Fairlie, T.D., Jacob, D.J., Park, R.J., 2007. The impact of transpacific transport of mineral dust in the United States. Atmos. Environ 41, 1251–1266.

Fountoukis, C., Nenes, A., 2007. ISORROPIA II: a computationally efficient thermodynamic equilibrium model for K^+–Ca^{2+}–Mg^{2+}–NH_4^+–Na^+–SO_4^{2-}–NO_3^-–Cl^-–H_2O aerosols. Atmos. Chem. Phys. 7, 4639–4659.

Fu, T.M., Cao, J.J., Zhang, X.Y., Lee, S.C., Zhang, Q., Han, Y.M., Qu, W.J., Han, Z., Zhang, R., Wang, Y.X., Chen, D., Henze, D.K., 2012. Carbonaceous aerosols in China: top-down constraints on primary sources and estimation of secondary contribution. Atmos. Chem. Phys. 12, 2725–2746. http://dx.doi.org/10.5194/acp-12-2725-2012.

Gu, J.X., Bai, Z.P., Li, W.F., Wu, L.P., Liu, A.X., Dong, H.Y., Xie, Y.Y., 2011. Chemical composition of $PM_{2.5}$ during winter in Tianjin, China. Particuology 9, 215–221.

Guenther, A., Karl, T., Harley, P., Wiedinmyer, C., Palmer, P.I., Geron, C., 2006. Estimates of global terrestrial isoprene emissions using MEGAN (Model of Emissions of Gases and Aerosols from Nature). Atmos. Chem. Phys. 6, 3181–3210.

Harrison, R.M., Collins, G.M., 1998. Measurements of reaction coefficients of NO_2 and HONO on aerosol particles. J. Atmos. Chem. 30, 397–406.

Henze, D.K., Seinfeld, J.H., 2006. Global secondary organic aerosol from isoprene oxidation. Geophys. Res. Lett. 33, L09812. http://dx.doi.org/10.1029/2006GL025976.

Henze, D.K., Seinfeld, J.H., Ng, N.L., Kroll, J.H., Fu, T.M., Jacob, D.J., Heald, C.L., 2008. Global modeling of secondary organic aerosol formation from aromatic hydrocarbons: high- vs. low-yield pathways. Atmos. Chem. Phys. 8, 2405–2421.

Huang, X., Song, Y., Li, M., Li, J., Huo, Q., Cai, X., Zhu, T., Hu, M., Zhang, H., 2012. A high-resolution ammonia emission inventory in China. Global Biogeochem. Cycle 26, GB1030. http://dx.doi.org/10.1029/2011GB004161.

IPCC, 2007. Climate change 2007: the physical science basis. In: Solomon, S., et al. (Eds.), Contribution of Working Group I to the Fourth Assessment Report of the Intergovernmental Panel on Climate Change. Cambridge University Press, Cambridge, United Kingdom and New York, pp. 1–996.

Jacob, D.J., 2000. Heterogeneous chemistry and tropospheric ozone. Atmos. Environ. 34, 2131–2159.

Li, J., Wang, Z.F., Wang, X., Yamaji, K., Takigawa, M., Kanaya, Y., Pochanart, P., Liu, Y., Irie, H., Hu, B., Tanimoto, H., Akimoto, H., 2011. Impacts of aerosols on summertime tropospheric photolysis frequencies and photochemistry over Central Eastern China. Atmos. Environ. 45, 1817–1829.

Liao, H., Henze, D.K., Seinfeld, J.H., Wu, S.L., Mickley, L.J., 2007. Biogenic secondary organic aerosol over the United States: comparison of climatological simulations with observations. J. Geophys. Res. 112, D06201. http://dx.doi.org/10.1029/2006JD007813.

Liao, H., Seinfeld, J.H., 2005. Global impacts of gas-phase chemistry–aerosol interactions on direct radiative forcing by anthropogenic aerosols and ozone. J. Geophys. Res. 110, D18208. http://dx.doi.org/10.1029/2005JD005907.

Liao, H., Yung, Y.L., Seinfeld, J.H., 1999. Effects of aerosols on tropospheric photolysis rates in clear and cloudy atmospheres. J. Geophys. Res. 104 (D19), 23,697–23,707.

Lin, W., Xu, X., Zhang, X., Tang, J., 2008. Contributions of pollutants from North China Plain to surface ozone at the Shangdianzi GAW station. Atmos. Chem. Phys. 8, 5889–5898.

Liu, X.-H., Zhang, Y., Xing, J., Zhang, Q., Wang, K., Streets, D.G., Jang, C., Wang, W.-X., Hao, J.-M., 2010. Understanding of regional air pollution over China using CMAQ, part II. Process analysis and sensitivity of ozone and particulate matter to precursor emissions. Atmos. Environ. 44, 3719–3727.

Macintyre, H.L., Evans, M.J., 2010. Sensitivity of a global model to the uptake of N_2O_5 by tropospheric aerosol. Atmos. Chem. Phys. 10, 7409–7414. http://dx.doi.org/10.5194/acp-10-7409-2010.

Mao, J., Fan, S., Jacob, D.J., Travis, K.R., 2013. Radical loss in the atmosphere from Cu–Fe redox coupling in aerosols. Atmos. Chem. Phys. 13, 509–519. http://dx.doi.org/10.5194/acp-13-509-2013.

Martin, R.V., Jacob, D.J., Yantosca, R.M., 2003. Global and regional decreases in tropospheric oxidants from photochemical effects of aerosols. J. Geophys. Res. 108, (D3), 4097. http://dx.doi.org/10.1029/2002JD002622.

Park, R.J., Jacob, D.J., Chin, M., Martin, R.V., 2003. Sources of carbonaceous aerosols over the United States and implications for natural visibility. J. Geophys. Res. 108 (D12), 4355. http://dx.doi.org/10.1029/2002JD003190.

Park, R.J., Jacob, D.J., Field, B.D., Yantosca, R.M., Chin, M., 2004. Natural and transboundary pollution influences on sulfate-nitrate-ammonium aerosols in the United States: implications for policy. J. Geophys. Res 109, D15204. http://dx.doi.org/10.1029/2003JD004473.

Pozzoli, L., Bey, I., Rast, S., Schultz, M.G., Stier, P., Feichter, J., 2008. Trace gas and aerosol interactions in the fully coupled model of aerosol-chemistry-climate ECHAM5-HAMMOZ: 1. Model description and insights from the spring 2001 TRACE-P experiment. J. Geophys. Res. 113, D07308. http://dx.doi.org/10.1029/2007JD009007.

Pye, H.O.T., Liao, H., Wu, S., Mickley, L.J., Jacob, D.J., Henze, D.K., Seinfeld, J.H., 2009. Effect of changes in climate and emissions on future sulfate–nitrate–ammonium aerosol levels in the United States. J. Geophys. Res. 114, D01205. http://dx.doi.org/10.1029/2008JD010701.

Real, E., Sartelet, K., 2011. Modeling of photolysis rates over Europe: impact on chemical gaseous species and aerosols. Atmos. Chem. Phys. 11, 1711–1727. http://dx.doi.org/10.5194/acp-11-1711-2011.

Rudich, Y., Talukdar, R.K., Ravishankara, A.R., Fox, R.W., 1996. Reactive uptake of NO_3 on pure water and ionic solutions. J. Geophys. Res. 101, 21,023–21,231.

Sander, S.P., Friedl, R.R., Barker, J.R., Golden, D.M., Kurylo, M.J., Wine, P.H., Abbatt, J.P.D., Burkholder, J.B., Kolb, C.E., Moortgat, G.K., Huie, R.E., Orkin, V.L., 2003. Chemical Kinetics and Photochemical Data for Use in Atmospheric Studies, Evaluation Number 14. JPL Publication, pp. 02–25. Jet Propul. Lab. Calif. Inst. Technol. Pasadena. Available at: http://jpldataeval.jpl.nasa.gov/pdf/JPL_02-25_rev02.pdf.

Seinfeld, J.H., Pandis, S.N., 2006. Atmospheric Chemistry and Physics, second ed. John Wiley: A Wiley-Interscience Publication Press.

Streets, D.G., Bond, T.C., Carmichael, G.R., Fernandes, S.D., Fu, Q., He, D., Klimont, Z., Nelson, S.M., Tsai, N.Y., Wang, M.Q., Woo, J.-H., Yarber, K.F., 2003. An inventory of gaseous and primary aerosol emissions in Asia in the year 2000. J. Geophys. Res. 108 (D21), 8809. http://dx.doi.org/10.1029/2002JD003093.

Takami, A., Wang, W., Tang, D.G., Hatakeyama, S., 2006. Measurements of gas and aerosol for two weeks in northern China during the winter–spring period of 2000, 2001 and 2002. Atmos. Res. 82, 688–697.

Tang, Y., Carmichael, G.R., Kurata, G., Uno, I., Weber, R.J., Song, C.H., Guttikunda, S.K., Woo, J.H., Streets, D.G., Wei, C., Clarke, A.D., Huebert, B., Anderson, T.L., 2004. Impacts of dust on regional tropospheric chemistry during the ACE-Asia experiment: a model study with observations. J. Geophys. Res 109, D19S21. http://dx.doi.org/10.1029/2003JD003806.

Thornton, J.A., Braban, C.F., Abbatt, J.P.D., 2003. N_2O_5 hydrolysis on sub-micron organic aerosol: the effect of relative humidity, particle phase and particle size. Phys. Chem. Chem. Phys. 5 (20), 4593–4603.

Thornton, J.A., Jaegle, L., McNeill, V.F., 2008. Assessing known pathways for HO_2 loss in aqueous atmospheric aerosols: regional and global impacts on tropospheric oxidants. J. Geophys. Res 113, D05303. http://dx.doi.org/10.1029/2007JD009236.

Tie, X.X., Madronich, S., Walters, S., Edwards, D.P., Ginoux, P., Mahowald, N., Zhang, R.Y., Lou, C., Brasseur, G., 2005. Assessment of the global impact of aerosols on tropospheric oxidants. J. Geophys. Res 110, D03204. http://dx.doi.org/10.1029/2004JD005359.

Tu, J., Xia, Z., Wang, H., Li, W., 2007. Temporal variations in surface ozone and its precursors and meteorological effects at an urban site in China. Atmos. Res. 85, 310–337.

Wang, T., Wei, X.L., Ding, A.J., Poon, C.N., Lam, K.S., Li, Y.S., Chan, L.Y., Anson, M., 2009. Increasing surface ozone concentrations in the background atmosphere of Southern China, 1994–2007. Atmos. Chem. Phys. 9, 6217–6227.

Wang, T., Wong, C.H., Cheung, T.F., Blake, D.R., Arimoto, R., Baumann, K., Tang, J., Ding, G.A., Yu, X.M., Li, Y.S., Streets, D.G., Simpson, I.J., 2004. Relationships of trace gases and aerosols and the emission characteristics at Lin'an, a rural site in eastern China, during spring 2001. J. Geophys. Res 109, D19S05. http://dx.doi.org/10.1029/2003JD004119.

Wang, T., Wong, H.L.A., Tang, J., Ding, A., Wu, W.S., Zhang, X.C., 2006. On the origin of surface ozone and reactive nitrogen observed at a remote mountain site in the northeastern Qinghai–Tibetan Plateau, western China. J. Geophys. Res. 111, D08303. http://dx.doi.org/10.1029/2005JD006527.

Wang, Y., Zhang, Y., Hao, J., Luo, M., 2011. Seasonal and spatial variability of surface ozone over China: contributions from background and domestic pollution. Atmos. Chem. Phys. 11, 3511–3525.

Wang, Y., Zhang, Q.Q., He, K., Zhang, Q., Chai, L., 2013. Sulfate-nitrate-ammonium aerosols over China: response to 2000–2015 emission changes of sulfur dioxide, nitrogen oxides, and ammonia. Atmos. Chem. Phys. 13, 2635–2652. http://dx.doi.org/10.5194/acp-13-2635-2013.

Wild, O., Akimoto, H., 2001. Intercontinental transport of ozone and its precursors in a three-dimensional global CTM. J. Geophys. Res. 106 (D21), 27,729–27,744.

Wild, O., Zhu, X., Prather, M.J., 2000. Fast-J: accurate simulation of in- and below-cloud photolysis in tropospheric chemical models. J. Atmos. Chem. 37, 245–282.

Xu, J., Zhang, Y.H., Zheng, S.Q., He, Y.J., 2012. Aerosol effects on ozone concentrations in Beijing: a model sensitivity study. J. Environ. Sci. 24 (4), 645–656.

Yan, P., Li, X., Luo, C., Xu, X., Xiang, R., Ding, G., Tang, J., Wang, M., Yu, X., 1997. Observational analysis of surface O_3, NO_x, and SO_2 in China. Appl. Meteor. 8 (1), 53–61 (in Chinese).

Yan, P., Wang, M., Cheng, H., Zhou, X.J., 2003. Distributions and variations of surface ozone in Changshu, Yangtze Delta region. Acta Metall. Sin. 17, 205–217.

Yang, G., Fan, S., Tang, J., Jin, S., Meng, Z., 2008. Characteristic of surface ozone concentrations at Lin'an. Res. Environ. Sci. 21 (3), 31–35 (in Chinese).

Zhang, L., Liao, H., Li, J.P., 2010. Impacts of Asian summer monsoon on seasonal and interannual variations of aerosols over eastern China. J. Geophys. Res. 115, D00K05. http://dx.doi.org/10.1029/2009JD012299.

Zhang, X.Y., Cao, J.J., Li, L.M., Arimoto, R., Cheng, Y., Huebert, B., Wang, D., 2002. Characterization of atmospheric aerosol over Xian in the south margion of the Loess Plateau, China. Atmos. Environ. 36, 4189–4199.

Zhang, X.Y., Wang, Y.Q., Niu, T., Zhang, X.C., Gong, S.L., Zhang, Y.M., Sun, J.Y., 2012. Atmospheric aerosol compositions in China: spatial/temporal variability, chemical signature, regional haze distribution and comparisons with global aerosols. Atmos. Chem. Phys 12, 779–799. http://dx.doi.org/10.5194/acp-12-779-2012.

Zhang, Y.H., Hu, M., Zhong, L.J., Widensohler, A., Liu, S.C., Andreae, M.O., Wang, W., Fan, S.J., 2008. Regional integrated experiments on air quality over Pearl River Delta 2004 (PRIDE-PRD2004): overview. Atmos. Environ. 42, 6157–6173.